

# Post-Newtonian templates for gravitational waves from compact binary inspirals

Soichiro Isoyama <sup>\*</sup>, Riccardo Sturani and Hiroyuki Nakano

**Abstract** To enable detection and maximise the physics output of gravitational wave observations from compact binary systems, it is crucial the availability of accurate waveform models. The present work aims at giving an overview for non-experts of the (inspiral) waveforms used in the gravitational wave data analysis for compact binary coalescence. We first provide the essential elements of gravitational radiation physics within a simple Newtonian orbital dynamics and the linearized gravity theory, describing the adiabatic approximation applied to binary systems: the key element to construct the theoretical gravitational waveforms in practice. We next lay out the gravitational waveforms in the post-Newtonian approximation to General Relativity, and highlight the basic input for the inspiral waveform of the slowly evolving, spinning, nonprecessing, quasicircular binary black holes, namely, post-Newtonian energy, fluxes and the (absorption-corrected) balance equation. The post-Newtonian inspiral templates are then presented both in the time and frequency domain. Finally, including the merger and subsequent ringdown phase, we briefly survey the two families of the full waveform models of compact binary mergers currently implemented in LSC Algorithm Library Simulation: the effective-one-body approach and the phenomenological frequency domain model.

---

Soichiro Isoyama  
School of Mathematics, University of Southampton, Southampton, United Kingdom. e-mail: [isoyama@yukawa.kyoto-u.ac.jp](mailto:isoyama@yukawa.kyoto-u.ac.jp)

Riccardo Sturani  
International Institute of Physics, Universidade Federal do Rio Grande do Norte, Natal, Brazil.  
e-mail: [riccardo.sturani@ufrn.br](mailto:riccardo.sturani@ufrn.br)

Hiroyuki Nakano  
Faculty of Law, Ryukoku University, Kyoto, Japan. e-mail: [hinakano@law.ryukoku.ac.jp](mailto:hinakano@law.ryukoku.ac.jp)

<sup>\*</sup> corresponding author

## Keywords

Binary black holes, Compact object binaries, Gravitational waves, Post-Newtonian approximation, Adiabatic approximation, Stationary phase approximation, Inspiral-merger-ringdown waveforms, LSC Algorithm Library.

## Introduction

The recent detection of gravitational waves (GW) from compact binary coalescences made by the large interferometers LIGO [1] and Virgo [19] opened the era of GW astronomy, triggering scientific interests over all aspects of GW production and detection. This new, exciting branch of scientific activity is even bursting now, with the third GW interferometer: KAGRA online [27]; for a useful summary of these detectors see Chapter 2 by Grote and Dooley in this book.

Because the GW signals are in general drowned in a much larger noise, their extraction from data stream and correct interpretation crucially depend on the quality of theoretically predicted template waveforms. Experimental data are processed via matched-filtering techniques; see, e.g., Ref. [28], which are particularly sensitive to the *phase* of GW signals; hence, a prediction of waveforms with absolute  $\ll \mathcal{O}(1)$  precision (in the phase) is very important, especially for a correct parameter estimation and in general for maximising the physics output of detection (see, e.g., Chapter 43 by Krolak in this book for differences between GW searches and parameter estimations).

From the point of view of theoretical modelling, the process of binary coalescence can be divided into three distinct phases: inspiral, merger and ringdown. During the inspiral phase, due to large binary separation with respect to their size, the dynamics can be efficiently described within the post-Newtonian (PN) approximation to general relativity (GR), the small expansion parameter being

$$\frac{GM}{c^2 R} \sim \frac{v^2}{c^2} \ll 1, \quad (1)$$

where  $M$ ,  $v$ , and  $R$  denote, respectively, the total mass, characteristic orbital velocity, and characteristic separation of the binary system. A  $n$ -PN correction to the gravitational potential is then given by any term of the type  $(M/R)^{n-j} v^{2j}$  with integers  $0 \leq j \leq n$ . The GR corrections to the Newtonian dynamics around flat Minkowski spacetime are then incorporated into the equation of motion and Einstein's field equations (expanded around the Minkowski metric) order by order in that small parameter. An excellent textbook devoted to the PN theory is *Gravity* by Poisson and Will [157]; more expert-oriented reviews (including more recent developments) are provided by Blanchet [42], Schäfer and Jaranowski [169], and Futamase and Itoh [88]. Recently, the PN approximation to GR has been developed in an effective field theory description [92], dubbed non-relativistic GR (NRGR), which resulted

in an alternative, independent and equivalent derivation of the PN dynamics (see Refs. [91, 84, 158, 123] for reviews, and Chapter 32 by Sturani in this book).

It is a remarkable feature of GR that the two-body dynamics in the inspiral phase is exactly the one of two (structureless) point particles up to 5PN when finite finite-size effects come into play, according to the *effacement principle* [64]. However, finite size effects that tidally “deform” a black hole (BH) have been shown to vanish for a spherical, non-spinning BHs [41, 69, 115, 94] in the static limit, and there are indications that they vanish for spinning BHs, too [155, 151] (see also [121, 59? ]). On the other hand the tidal deformation effects for *material* bodies like neutron stars (NS) are expected, depending on the equation of state of matter in NSs, and there have been some evidence of their detection in GW170817 [11].

Considering circular orbit, in the nonprecessing case, is usually accurate since angular momentum radiation is more efficient than energy radiation; thus, binary orbits tend to circularize at early stage [152]. However, while unlikely, it is not excluded that some observed GW signals can show a non-negligible eccentricity due to, e.g., dynamical formation of binary BHs (BBHs) presented in Chapter 15 by Kocsis in this book. When spins are included in the binary dynamics, in general, one has to also take into account orbital precession caused by the orbital angular momentum-spin coupling, as well as the relativistic precession of the spins.

As the binary’s orbital separation shrinks by decreasing the binding energy through the emission of GWs (with an increase in relative velocity of the constituents), the system enters the merger phase where two compact objects form one single object. At the merger phase the PN approximation breaks down,  $v \lesssim 1$ , and full numerical-relativistic simulations have to be used, where the nonlinear radiative dynamics of the binaries is obtained by directly solving the exact Einstein field equations numerically: see, e.g., a recent text by Baumgarte and Shapiro [34] and Chapter 34 by Zhao et al. in this book. Immediately after the merger a perturbed BH forms which rapidly damps its excitation in a ringdown phase, whose GW emission is described by a superposition of damped sinusoids [146, 114, 39]; the detail can be found in Chapter 38 by Konoplya in this book.

Current inspiral-merger-ringdown (IMR) waveform models for data analysis applications combine input from the PN theory and NR simulations. The models implemented in the LSC Algorithm Library (LAL) Simulation [126] are summarized in “Enumeration Type Documentation” in Ref. [61]. The GW signal models used for the analyses of observed GW events so far are described in:

GW150914: first BBH detection [8, 9],

GW170817: first binary NS (BNS) detection [11, 4],

events from the first Gravitational Wave Transient Catalog: first and second observation runs, O1 and O2 henceforth, including the above two GW events, along with GW151012, GW151226, GW170104, GW170608, GW170729, GW170809, GW170814, GW170818, GW170823 [3],

GW190412: O3, unequal mass (mass ratio  $\sim 3$  with nonzero spin for the heavier object) BBH [13],

GW190425: O3, second BNS detection [7],

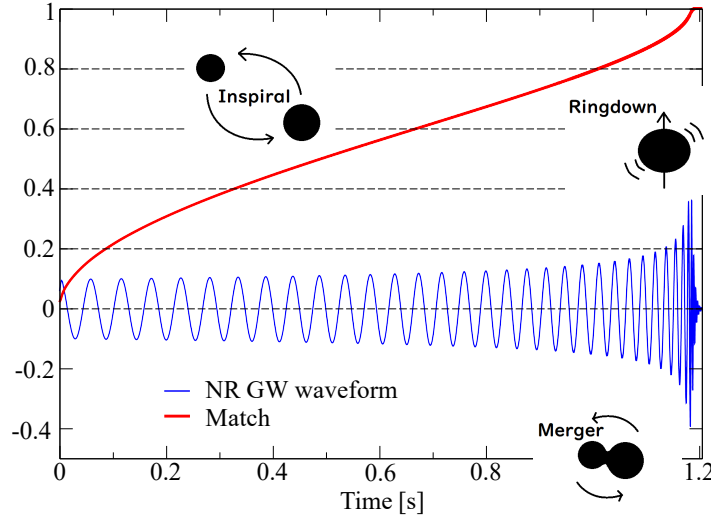


**Fig. 1** Inspiral-merger-ringdown (IMR) signal from the numerical-relativity simulation SXS:BBH:0305 [47] which models GW150914. The horizontal axis is the real time. Here, we present only the (scaled) “+” GW mode (blue thin curve). The red thick curve shows the “match”, i.e. the accumulation of the (normalized) signal-to-noise ratio in white noise.

GW190814: O3, highest mass ratio between binary constituents ( $\sim 10$ ) and lighter object in the low “mass gap” [15],

GW190521: O3, whose remnant can be considered as the first ever evidence of a light intermediate mass ( $\sim 10^2 M_\odot$ ) BH [14, 16],  
 events from the second Gravitational Wave Transient Catalog: the first half of the third observing run (O3a), including 39 GW events [18].

### *Goal and relation to other chapters*

Our purpose with this chapter is twofold: (i) to make a compilation of the PN-based GW waveform models for the binary inspirals in literature; (ii) to provide a “catalogue” of IMR waveform families implemented in the LALSimulation. The main target audience is graduate students (as well as researchers) who work in areas outside of the GW source modelling of binaries, but who need a working knowledge of waveform models.

We set the stage with the basics of gravitational radiation physics, using the simple quadrupole formalism in the linearized gravity theory. We next cover the GW waveforms in the PN theory, collecting the state of art of PN binding energy and energy flux of slowly evolving, spinning, and nonprecessing BBHs, and present their inspiral PN templates both in the time and frequency domains. Then, we briefly overview the two main families of the full IMR waveforms: the effective-

one-body approach and the phenomenological frequency-domain model, used and implemented in LALSimulation so far. We conclude our chapter with some of remaining issues and future prospects.

### **Notations**

We use the metric signature  $(-+++)$  and the standard geometrized unit ( $c = 1 = G$ ) with the useful conversion factor  $1M_{\odot} = 1.477 \text{ km} = 4.926 \times 10^{-6} \text{ s}$ , throughout. Greek indices  $\mu, \nu, \dots$  denote 0, 1, 2, 3 (or, e.g.,  $t, x, y, z$ ) while the Latin letters  $i, j, \dots$  run over 1, 2, 3.

For a binary with masses  $m_a$  and spin vector  $\mathbf{S}_a$  (where  $a = 1, 2$  labels each compact object), we will use the notation defined in Ref. [3]. The total mass of a binary is

$$M \equiv m_1 + m_2, \quad (2)$$

and the mass ratio is

$$q \equiv \frac{m_2}{m_1} \leq 1. \quad (3)$$

We also use the symmetric mass ratio

$$\eta \equiv \frac{m_1 m_2}{M^2}, \quad (4)$$

and the reduced mass  $\mu \equiv \eta M$ . The spin vector  $\mathbf{S}_a$  has a conserved magnitude, as long as absorption effects are neglected, by using an appropriate spin supplementary condition to remove unnecessary degrees of freedom associated with the spin, and we denote its dimensionless magnitude by

$$\chi_a \equiv |\boldsymbol{\chi}_a| \equiv \frac{|\mathbf{S}_a|}{m_a^2}. \quad (5)$$

Finally, the  $O(v^{2n})$  terms relative to the Newtonian dynamics will be referred to as the  $n$ -th PN order.

### **The essence: Quadrupole radiation from a mass in circular orbit**

The essence of GW generation formalism for a binary inspiral can be understood from the Newtonian orbital dynamics and the Einstein's quadrupole formalism based on the linearized gravity theory. While a raw approximation, the linearized gravity theory catches the basic concepts behind the GW signal calculation, without the intricacies of the full GR nonlinearity (see, e.g., Chapter 11 of Poisson and Will [157] for rigorous derivation of the quadrupole formula and details about the PN treatment). We here review the main line of reasoning and results, modelled on

nice tutorials by Flanagan and Hughes [83] and the LVC collaboration [12]. The material covered in this section is fairly standard, and the details of derivation are given in various introductory GW and GR texts, including Landau and Lifshitz [119] and Maggiore [129].

We start by supposing that the full spacetime metric (i.e., gravitational field)  $g_{\mu\nu}$  deviates only slightly from the background flat metric  $\eta_{\mu\nu} \equiv \text{diag}(-1, 1, 1, 1)$ :

$$g_{\mu\nu} = \eta_{\mu\nu} + h_{\mu\nu}, \quad ||h_{\mu\nu}|| \ll 1, \quad (6)$$

where  $h_{\mu\nu}$  is a small metric perturbation (i.e., weak gravitational field) of the background Minkowski spacetime, and  $||h_{\mu\nu}||$  is a typical magnitude of  $h_{\mu\nu}$ .

In the linearized gravity theory, everything is consistently expanded to linear order in  $h_{\mu\nu}$ , neglecting all higher-order terms, and all indices are raised and lowered with the Minkowski metric  $\eta_{\mu\nu}$ . Also, we assume that the decomposition of the metric (6) is always preserved in any coordinate system that we can chose. The general covariance of full GR is then restricted to an infinitesimal coordinate transformation

$$x'^{\mu} = x^{\mu} + \xi^{\mu}, \quad (7)$$

where  $\xi^{\mu}(x)$  is an infinitesimal vector field, and the metric perturbation changes via

$$h'_{\mu\nu} = h_{\mu\nu} - \partial_{\mu}\xi_{\nu} - \partial_{\nu}\xi_{\mu}. \quad (8)$$

(Note the close analogy to the gauge transformation of the vector potential  $A^{\mu}$  in electromagnetic theory, i.e.,  $A'_{\mu} = A_{\mu} - \partial_{\mu}\chi$  with a scalar field  $\chi$ . This is why Eq. (8) is often referred to as a gauge transformation in the linearized gravity theory).

The Einstein's field equations in the linearized theory are best described under the Lorenz-gauge conditions

$$\partial^{\mu}\bar{h}_{\mu\nu} = 0, \quad (9)$$

in terms of the trace-reversed perturbation

$$\bar{h}_{\mu\nu} \equiv h_{\mu\nu} - \frac{1}{2}\eta_{\mu\nu}h^{\rho}_{\rho}, \quad (10)$$

which can be enforced without loss of generality by making use of the coordinate freedom (8). The Lorenz-gauge conditions reduce the Einstein's equations to a simple, decoupled wave equation for  $\bar{h}_{\mu\nu}$  given by

$$\square\bar{h}_{\mu\nu} = -16\pi T_{\mu\nu}, \quad (11)$$

where  $\square \equiv \partial^{\mu}\partial_{\mu}$  is the d'Alembertian operator, and  $T_{\mu\nu}$  is the energy-momentum tensor of the matter. Equation (11) can be solved by the method of Green's function  $G(x, x')$  (for the operator  $\square$ ), imposing suitable boundary conditions. For the problem of the GW radiation, just like in electromagnetism, the appropriate choice is the retarded Green's function:

$$G(x, x') = -\frac{1}{4\pi} \frac{\delta(t' - t_{\text{ret}})}{|\mathbf{x} - \mathbf{x}'|}, \quad (12)$$

where  $t_{\text{ret}} \equiv t - |\mathbf{x} - \mathbf{x}'|$  is the retarded time, accounting for the propagation delay between the source at  $\mathbf{x}'$  and the observer at  $\mathbf{x}$ . The associated retarded solution of Eq. (11) is then given by

$$\bar{h}_{\mu\nu} = 4 \int d^3x' \frac{T_{\mu\nu}(t - |\mathbf{x} - \mathbf{x}'|, \mathbf{x}')}{|\mathbf{x} - \mathbf{x}'|}. \quad (13)$$

For the GW calculation, again like the radiation in the electromagnetism, we are particularly interested in the behavior of the solution (11) in the (far-away) wave zone, where the length of the position vector  $r \equiv |\mathbf{x}|$  is larger than the characteristic wavelength of the GW radiation  $\lambda_{\text{Char}}$  (defined by  $\lambda_{\text{Char}} = t_{\text{Char}}$  in terms of the characteristic time scale of the change in the source  $t_{\text{Char}}$ ). The characteristic radius  $r_{\text{Char}} \sim v t_{\text{Char}}$  of the matter distribution is then smaller than  $\lambda_{\text{Char}}$ , justifying the expansion  $|\mathbf{x} - \mathbf{x}'| = r - n^i x'_i + O(r_{\text{Char}}^2/r)$  with  $n^i \equiv x^i/r$ , the zero-th solution in the (far-away) wave zone is given by

$$\bar{h}_{\mu\nu} = \frac{4}{r} \int d^3x' T_{\mu\nu}(t - r, \mathbf{x}'). \quad (14)$$

Here, not only the terms that fall off as  $O(1/r^2)$  and higher are neglected, but there is an additional approximation: all elements of the extended source contribute to field at the same retarded time.

At this point, we must identify the truly radiative degrees of freedom contained in Eq. (14). Apparently, all six degrees of freedom in  $h_{\mu\nu}$  ( $h_{\mu\nu}$  have ten components, and four are constrained by the Lorenz-gauge condition (9)) look radiative. However, they are not; only two are actually radiative. The remaining four are non-radiative degrees of freedom tied to the matter (like the Coulomb piece of the electromagnetic field), and their wave-like behaviours are merely artefact due to the Lorenz-gauge formulation of linearized Einstein equation (11). Indeed, a detailed analysis of the linearized gravity theory by Flanagan and Hughes [83] reveals that the radiative degrees of freedom are just encoded in the spatial transverse-traceless components  $h_{ij}^{\text{TT}}$  of  $h_{\mu\nu}$ , which satisfies the following four conditions (in addition to the Lorenz gauge condition):

$$\partial^i h_{ij}^{\text{TT}} = 0, \quad h_i^{\text{TT}} = 0. \quad (15)$$

Importantly,  $h_{ij}^{\text{TT}}$  is coordinate-invariant (gauge-invariant) under the transformation (8) (as long as the full metric (6) remains asymptotically flat), and hence, it is the direct observable of GW detectors, e.g., LIGO, Virgo, and KAGRA. In the (far-away) wave zone,  $h_{ij}^{\text{TT}}$  can be obtained by projecting  $h_{\mu\nu}$  onto the plane orthogonal to the direction of propagation  $\mathbf{n} = \mathbf{x}/r$  and subtracting its trace. We introduce the projector (this is sometimes referred to as Lambda tensor [129])

$$\Lambda_{ij,kl} \equiv P_{ik}P_{jl} - \frac{1}{2}P_{ij}P_{kl}, \quad (16)$$

where  $P_{ij} = \delta_{ij} - n_i n_j$ , and we obtain

$$\bar{h}_{ij}^{\text{TT}} = \frac{4}{r} \Lambda_{ij,kl} \int d^3x' T^{kl}(t-r, \mathbf{x}'). \quad (17)$$

For the final step, we simplify the integral on the right of Eq. (17), making use of the energy-momentum conservation  $\partial_\mu T^{\mu\nu} = 0$  repeatedly to obtain the convenient relation

$$2 \int d^3x' T^{ij} = \partial_i^2 \left( \int d^3x' T^{00} x^i x^j \right). \quad (18)$$

Defining a (Newtonian) symmetric trace-free quadrupole moment by

$$Q_{ij}(t) \equiv \int d^3x' \rho(t, \mathbf{x}') \left( x^i x^j - \frac{1}{3} \delta_{ij} \mathbf{x}'^2 \right), \quad (19)$$

where  $\rho \equiv T^{00}$  is the Newtonian mass density and  $\delta_{ij} \equiv \text{diag}(1, 1, 1)$  is the Kronecker-delta. Inserting Eq. (19) back into Eq. (17), we arrive at

$$h_{ij}^{\text{TT}}(t, \mathbf{x}) = \frac{2}{r} \Lambda_{ij,kl}(\mathbf{n}) \frac{d^2 Q_{kl}}{dt^2}(t-r). \quad (20)$$

This is the well-known ‘‘quadrupole formula’’ for the GW signal.

The two radiative degrees of freedom contained in  $h_{ij}^{\text{TT}}$  can be conveniently extracted by introducing two unit polarization vectors  $\mathbf{p}$  and  $\mathbf{q}$ , which are orthogonal to the propagation direction  $\mathbf{n}$  and to each other (satisfying  $n_i n_j + p_i p_j + q_i q_j = \delta_{ij}$ ). The tensor  $h_{ij}^{\text{TT}}$  is then decomposed into two independent ‘‘plus’’ and ‘‘cross’’ polarization modes of GWs:

$$h_{ij}^{\text{TT}} = h_+(p_i p_j - q_i q_j) + h_\times(p_i q_j + q_i p_j). \quad (21)$$

For example, if we use a Cartesian coordinate system  $\mathbf{x} = (x, y, z)$ ,  $h_+$  and  $h_\times$  modes of GWs that propagate in the  $z$ -direction (so that  $\mathbf{n} = (0, 0, 1)$ ) are

$$\begin{aligned} h_+(t, z) &= \frac{1}{r} \left( \frac{d^2 Q_{xx}}{dt^2} - \frac{d^2 Q_{yy}}{dt^2} \right), \\ h_\times(t, z) &= \frac{2}{r} \frac{d^2 Q_{xy}}{dt^2}. \end{aligned} \quad (22)$$

We now apply the GW polarization modes (22) to the Newtonian binary system in a fixed circular orbit with the separation  $R$  and the orbital frequency  $\Omega$  (we will momentarily delay to discuss the back-reaction on the motion due to the GW emission from the system). To compute the quadrupole moment  $Q_{ij}$ , we continue to use the Cartesian coordinate system and assume that the orbit lies in the  $x$ - $y$  plane whose center of mass is at the coordinate origin. In this setup, we have



$$Q_{ij} = \mu \left( x_i x_j - \frac{R^2}{3} \delta_{ij} \right) \quad (23)$$

with  $x = R \cos(\Omega t + \pi/2)$ ,  $y = R \sin(\Omega t + \pi/2)$  and  $z = 0$  (so that the binary initially at  $x(0) = 0$  and  $y(0) = R$  when  $t = 0$ ). The second derivative of Eq. (23) is

$$\begin{aligned} \frac{d^2 Q_{xx}}{dt^2} &= 2\mu R^2 \Omega^2 \cos(2\Omega t) = -\frac{d^2 Q_{yy}}{dt^2}, \\ \frac{d^2 Q_{xy}}{dt^2} &= 2\mu R^2 \Omega^2 \sin(2\Omega t). \end{aligned} \quad (24)$$

Making substitution in Eq. (22), we obtain

$$\begin{aligned} h_+(t) &= \frac{4\mu}{r} (\Omega R)^2 \cos(2\Omega t_{\text{ret}}), \\ h_\times(t) &= \frac{4\mu}{r} (\Omega R)^2 \sin(2\Omega t_{\text{ret}}), \end{aligned} \quad (25)$$

where the retarded time  $t_{\text{ret}} \equiv t - r$  has been introduced. We notice that the quadrupole radiation is at twice the orbital frequency  $\Omega$ .

From the observational point of view, the GW detector only sees the radiation in the direction that points from the binary to the detector, and it is not always the same as  $z$ -direction like Eq. (25) in general. When the GW propagates in a direction of the line of sight to the binary  $n_i \equiv (\sin \theta \sin \phi, \sin \theta \cos \phi, \cos \theta)$ , the GW polarization that an observer measures is conveniently rewritten in the form (see, e.g., Chapter 3 of Maggiore [129])

$$\begin{aligned} h_+(t) &= \frac{4}{r} \mathcal{M}^{5/3} \Omega^{2/3} \left( \frac{1 + \cos^2 \theta}{2} \right) \cos(2\Omega t_{\text{ret}} + 2\phi), \\ h_\times(t) &= \frac{4}{r} \mathcal{M}^{5/3} \Omega^{2/3} \cos \theta \sin(2\Omega t_{\text{ret}} + 2\phi), \end{aligned} \quad (26)$$

where we use the Kepler's law for the circular orbit frequency  $\Omega^2 = M/R^3$ . Here, the combination of body's mass, the chirp mass:  $\mathcal{M}$ , is defined by

$$\mathcal{M} \equiv \eta^{3/5} M. \quad (27)$$

We remark that the amplitudes of the GW polarization at fixed  $\Omega$  depend on the binary masses only through the chirp mass  $\mathcal{M}$  (within the quadrupole approximation).

### ***Adiabatic approximation***

Our discussion has so far assumed that the GW is emitted from a given, fixed, (Newtonian) circular orbit. However, GW can transport energy, momentum, and angular

momentum away from the binary, and hence the GW radiation actually drives an evolution of the circular orbit at the same time; the orbital separation  $R$  will slowly shrink, causing the gradual radiative inspiral of the binary. In this subsection, we improve the GW signals (26), accounting for the inspiral motion of the binary due to the radiative losses.

The total radiated power in all directions around the binary (i.e., the total energy flux of GWs) that results from the quadrupole GW signal (20) is in general given by (see, e.g., Chapter 12 of Poisson and Will [157] for a derivation)

$$F_{\infty}^{\text{Newt}} = \frac{1}{5} \sum_{i,j=1}^3 \left\langle \frac{d^3 Q_{ij}}{dt^3} \frac{d^3 Q_{ij}}{dt^3} \right\rangle, \quad (28)$$

where  $\langle \dots \rangle$  stand for time average, which is well-known as the quadrupole (“Newtonian”) formula for the GW energy flux. Inserting here the quadrupole moment of the circular binaries (23), we obtain

$$F_{\infty}^{\text{Newt}} = \frac{32}{5} \eta^2 v^{10}, \quad (29)$$

where  $v \equiv \sqrt{M/R} = (M\Omega)^{1/3}$  is the (relative) orbital velocity.

We now assume the so-called adiabatic approximation, in which a circular orbit evolves with a slowly changing orbital velocity  $v$ , so that its fractional change over an orbital period is negligibly small. In this approximation, the source of the GW energy fluxes comes from the sum of the kinetic and the (Newtonian) binding energy of the binary

$$E^{\text{Newt}} = -\frac{M\eta}{2} v^2, \quad (30)$$

and hence it obeys the balance equation

$$\frac{dE^{\text{Newt}}}{dt} = -F_{\infty}^{\text{Newt}}. \quad (31)$$

The balance equation implies that the typical timescale of the radiation reaction is

$$t_{\text{RR}} \equiv \frac{E^{\text{Newt}}}{dE^{\text{Newt}}/dt} \sim M\eta^{-1} v^{-8}, \quad (32)$$

which is much longer than the orbital time scale

$$t_{\text{Orb}} \sim M v^{-3}, \quad (33)$$

as far as the orbital velocity is small (or, the orbital separation is large),  $v = \sqrt{M/R} \ll 1$ . Therefore, the adiabatic approximation is mostly valid during the inspiral phase of the orbital evolution, but it breaks down as the binary separation approaches to the last stable orbit (whose typical orbital radius is close to that of the Innermost Stable Circular Orbit (ISCO) in Schwarzschild geometry with the mass

$M$ ,  $r_{\text{ISCO}} = 6M$ ), where the transition from the inspiral phase to the merger phase approximately occurs.

In the adiabatic approximation, we can use the balance equation (31) to derive the evolution equation for any binary parameters. For instance, we have the evolution equation of the orbital velocity  $v(t)$ ,

$$\frac{dv}{dt} = \frac{32}{5} \frac{\eta}{M} v^9. \quad (34)$$

The time to coalescence  $t_c$  is formally defined by the time it takes the velocity to evolve from an initial value  $v_{\text{ini}}$  to  $v \rightarrow \infty$ , and it is

$$t_c = \frac{5}{256} \frac{M}{\eta v_{\text{ini}}^8} = \frac{5}{256} \left( \frac{R_{\text{ini}}}{M} \right)^4 \frac{(1+q)^2}{q} M, \quad (35)$$

where  $R_{\text{ini}} = M v_{\text{ini}}^{-2}$  denotes the initial orbital velocity and radius, respectively. Similarly, the differential equation

$$\frac{dR}{dt} = \left( \frac{dE}{dR} \right)^{-1} \frac{dE}{dt} = -\frac{64}{5} \frac{\eta M^2}{R^2}, \quad (36)$$

determines the shrinking rate of the orbital separation  $R(t)$ . Assuming  $r(t_c) = 0$ , we have the solution

$$R(t) = \left( \frac{256}{5} \eta M^3 \right)^{1/4} (t_c - t)^{1/4}. \quad (37)$$

In turn, recall the Kepler's third law  $\Omega^2 = M/R^3$ , it leads the increasing orbital frequency

$$\Omega(t) = \left( \frac{5}{256} \frac{1}{t_c - t} \right)^{3/8} \mathcal{M}^{-5/8}. \quad (38)$$

Importantly, the frequency evolution depends on the binary masses only through the chirp mass  $\mathcal{M}$  in the zero-th order approximation leading to Eq. (20).

We next wish to describe the impact of these time-dependent binary parameters on the GW signals (26) within the adiabatic approximation. Recall the discussion of the quadrupole GW generation formalism in the preceding subsection, the orbital frequency  $\Omega$  and the GW phase  $2\Omega t_{\text{ret}}$  have to be promoted to

$$\{\Omega, 2\Omega t_{\text{ret}}\} \rightarrow \{\Omega(t_{\text{ret}}), \phi(t_{\text{ret}})\}. \quad (39)$$

Here, we introduce a new accumulated phase of GW (associated with the time-dependent orbital frequency (38)) by

$$\phi(t) \equiv 2 \int \Omega(t) dt = -2 \left( \frac{1}{5} \frac{t_c - t}{\mathcal{M}} \right)^{5/8} + \phi_c, \quad (40)$$

and  $\phi_c \equiv \phi(t = t_c)$  is the phase at the time to coalescence  $t_c$ . Inserting Eq. (39) into Eq. (26), we arrive at

$$\begin{aligned} h_+(t) &= \frac{\mathcal{M}}{r} \left( \frac{5\mathcal{M}}{t_c - t} \right)^{1/4} \left( \frac{1 + \cos^2 \theta}{2} \right) \cos \left\{ -2 \left( \frac{1}{5} \frac{t_c - t}{\mathcal{M}} \right)^{5/8} + \phi_c \right\}, \\ h_\times(t) &= \frac{\mathcal{M}}{r} \left( \frac{5\mathcal{M}}{t_c - t} \right)^{1/4} \cos \theta \sin \left\{ -2 \left( \frac{1}{5} \frac{t_c - t}{\mathcal{M}} \right)^{5/8} + \phi_c \right\}. \end{aligned} \quad (41)$$

This is the GW polarization from inspiraling quasicircular binaries that an observer measures in a quadrupole approximation. Both the amplitudes and the frequency in Eq. (41) increase as the coalescence time is approached: this is referred to as “chirping” (in fact, the “chirp mass”  $\mathcal{M}$  is named after it), and we often call Eq. (41) the chirp signal. Also, we note that both the amplitude and the phase still depend on the binary masses only through the  $\mathcal{M}$ . This explains why the chirp mass is well determined in the GW data analysis, compared with the component masses of the binary,  $m_a$ .

### Stationary phase approximation

An alternative to the time-domain chirp signal (41) is its frequency-domain (i.e., Fourier domain) representation, which is also commonly used for the GW data analysis applications. The time-domain chirp signal takes the schematic complex-exponential form of  $h(t) = A(t)e^{-i\phi(t)}$ , and its Fourier transform is

$$\tilde{h}(f) = \int dt A(t) e^{i(2\pi ft - \phi(t))}; \quad (42)$$

note that  $\tilde{h}(-f) = \tilde{h}^*(f)$ , so we can assume  $f > 0$ . Since the amplitude of the chirp signal evolves much slower than the phase, i.e.,

$$\frac{d \ln A(t)}{dt} \ll \frac{d\phi(t)}{dt}, \quad (43)$$

the stationary phase approximation to the integral provides a good approximation of  $\tilde{h}(f)$ :

$$\tilde{h}(f) \simeq \frac{A(t)}{\sqrt{dF/dt(t_*)}} e^{i(\Psi_{\text{SPA}}(t_*) - \pi/4)}, \quad (44)$$

where

$$\Psi_{\text{SPA}}(t_*) \equiv 2\pi f t_* - \phi(t_*), \quad (45)$$

and  $t_*$  is a function of  $f$  defined as

$$\frac{d\phi(t_*)}{dt_*} \equiv 2\pi f, \quad (46)$$

and the time at the stationary point  $t_*$  is determined by the Fourier variable  $f$  being equal to the instantaneous frequency  $d\phi(t)/dt$  at  $t = t_*$ ,

The explicit calculation of the stationary phase approximation to the time-domain chirp signals (41) is worked out in, e.g., Chapter 4 of Maggiore [129]. The resultant frequency-domain chirp signal is

$$\begin{aligned}\tilde{h}_+(f) &= \frac{1}{\pi^{2/3}} \sqrt{\frac{5}{24}} \frac{\mathcal{M}^{5/6}}{f^{7/6}} \frac{e^{i\Psi_+(f)}}{r} \left( \frac{1 + \cos^2 \theta}{2} \right), \\ \tilde{h}_\times(f) &= \frac{1}{\pi^{2/3}} \sqrt{\frac{5}{24}} \frac{\mathcal{M}^{5/6}}{f^{7/6}} \frac{e^{i\Psi_\times(f)}}{r} \cos \theta,\end{aligned}\quad (47)$$

where the phases are given by

$$\begin{aligned}\Psi_+(f) &\equiv 2\pi f(t_c) - \phi_c - \frac{\pi}{4} + \frac{3}{128} (\pi \mathcal{M} f)^{-5/3}, \\ \Psi_\times(f) &\equiv \Psi_+(f) + \frac{\pi}{2}.\end{aligned}\quad (48)$$

## Post-Newtonian gravitational waveforms for spinning, nonprecessing binary black holes

In our discussion so far, we have restricted our analysis to the Newtonian orbital dynamics in the linearized gravity theory (with the quadrupole formula for the GW fluxes). While this treatment has provided an adequate description of the dynamics of the binary pulsars (e.g., the secular change in the orbital period of the Hulse-Taylor binary: PSR B1913+16; see a review [128]), it is not accurate modelling of the GW signals emitted from inspiralling astrophysical binary system; the chirp signals (41) are just inconsistent with the observed GW data of, e.g., BBHs GW150914 [8] and BNS GW170817 [11]. For the latter case, one must rely on an improved approximation method in GR to have a more refined wave-generation formalism.

The perfect starting point for that discussion is the ‘‘post-Newtonian (PN) theory,’’ applied to the two-body problem. The PN theory is a systematic approximation method to exact GR, solving the Einstein field equation (and the equation of the motion for a source) in the form of power series in small physical parameters

$$v \ll 1, \quad \frac{M}{R} \sim v^2 \ll 1, \quad (49)$$

namely, the two-body system is assumed to move slowly (with a large separation), and to be in the weak gravitational field. Therefore, the PN theory provides the most natural tool to model the early inspiral stage for LIGO-Virgo-KAGRA binary mergers.

The technical developments of the general wave-generation formalism in the PN theory is far more involved than the quadrupole moment formalism in the linearized theory, and we shall continue to specialise our discussion to GW signals emitted by a binary system in the (slowly evolving) circular orbit for simplicity. We refer the reader the text by Poisson and Will [157], Blanchet’s Living review article [42], and Chapter 32 by Sturani in this book for the effective field theory approach.

In the PN theory, the GW polarizations  $h_{+, \times}$  produced by a circular binary system have the following general structure ( $p$  is an integer number)

$$h_{+, \times} = \frac{2\mu v^2}{r} \sum_{p \geq 0} v^p H_{+, \times}^{(p)} + O\left(\frac{1}{r^2}\right), \quad (50)$$

where the variable  $v$  that was a relative orbital velocity in the previous section is conveniently redefined as the frequency-related parameter by

$$v^2 \equiv (M\Omega)^{2/3} = \frac{M}{R} \left\{ 1 + O\left(\frac{1}{c^2}\right) \right\}. \quad (51)$$

The leading-order terms of Eq. (50) explicitly reads (ignore the static non-linear memory contribution to  $H_+^{(0)}$ : see, e.g., Chapter 9 of Ref. [42])

$$H_+^{(0)} = -(1 + \cos^2 \theta) \cos 2\psi, \quad H_\times^{(0)} = -2 \cos \theta \sin 2\psi. \quad (52)$$

Here, we introduce the “tail-distorted” phase,

$$\psi = \phi(t) - 6v^3 \ln v, \quad (53)$$

where the binary’s orbital phase  $\phi(t)$  receives a correction from the scattering of the GW off the static curvature generated by the binary itself, note that since  $\phi(t) \sim v^{-5}$  in the quadrupole approximation, see Eqs. (38) and (40), this is a relative  $v^8$  correction to the leading order.

It is convenient to decompose the GW polarizations (50) onto the (spin-weighted) spherical harmonic mode (see, e.g., Section 3.1 of Blanchet’s review [42]) when comparing the PN waveform with, e.g., the numerical-relativity waveform. This is often called GW modes  $h_{\ell m}$ , which is expressed as

$$h_+(t) - ih_\times(t) = \sum_{\ell=2}^{\infty} \sum_{m=-\ell}^{\ell} h_{\ell m}(t) {}_{-2}Y_{\ell m}(\theta, \phi), \quad (54)$$

where  ${}_{-2}Y_{\ell m}$  is the spin  $(-2)$ -weighted spherical harmonics, and we note that  $h_{\ell-m} = (-1)^\ell \bar{h}_{\ell m}$ . The dominant quadrupole GW modes  $(\ell, m) = (2, 2)$  is (see, e.g., Ref. [24])

$$h_{22} = \frac{8\mu}{r} \sqrt{\frac{\pi}{5}} v^2 e^{-i2\psi} + O\left(v^3, \frac{1}{r^2}\right), \quad (55)$$

and the other GW modes starts at  $O(v^3)$  or higher.

For the GW data analysis applications, the phasing of the GW signal is significantly more important than its amplitude due to the matched-filter searching of the GW signal. Thus, the (so named) “restricted” PN waveform [63] is commonly used, in which only leading term  $H_{+, \times}^{(0)}$  (or  $h_{22}$ ) of the waveform is retained, while all the PN correction to the orbital phase evolution  $\phi(t)$  in Eq. (53) are included. (we note, however, that the higher-order amplitude terms become more pronounced especially for precessing or unequal mass-ratio binaries, e.g., GW190412 [13]). Because the early inspiral phase of binary is in the adiabatic regime, where the typical radiation-reaction time scale is much longer than the typical orbital time scale  $t_{\text{Orb}}/t_{\text{RR}} \sim O(v^5) \ll 1$  (recall Eqs. (32) and (33)), the orbital phase evolution  $\phi(t)$  in the restricted PN approximation can be computed efficiently, making use of the adiabatic approximation discussed previously.

The orbital phase  $\phi(t)$  nonetheless has to be calculated up to a very-high-order PN term. The PN phase evolution can be parametrized by the following general structure (discard the constant phase):

$$\phi(v) = -\frac{1}{32\eta} \frac{1}{v^5} \left\{ 1 + O(v^2) + O(v^3) + O(v^4) + O(v^5) + \dots \right\}. \quad (56)$$

Because the leading term in  $\phi(v)$  scales like  $O(v^{-5})$ , one needs to compute the PN corrections at least 2.5PN order (or even higher order) to keep the absolute phase error to less than  $O(1)$ , which is needed for the effectiveness of the matched-filtering search.

Throughout the rest of this section, assuming the adiabatic approximation and making a further specialization to the BBHs with aligned spins and without orbital eccentricity, we will review how the orbital phase  $\phi(t)$  can be computed up to the 3.5PN order [106]; adding the neglected effects for other binary configurations will be discussed in the next section. In this simpler setup, we will just need i) the PN (center-of-mass) binding energy, ii) the energy flux emitted to the infinity and across the BH horizons, and iii) the certain balance equation associated with them, as inputs.

### ***PN binding energy, energy flux, and BH horizon flux***

We schematically express the 3.5PN corrections to the Newtonian (center-of-mass) binding energy (30) as

$$E \equiv -\frac{M\eta}{2} v^2 \left\{ E_{\text{NS}} + \frac{v^3}{M^2} E_{\text{SO}} + \frac{v^4}{M^4} E_{\text{SS}} + \frac{v^7}{M^6} E_{\text{SSS}} + O(v^8) \right\}, \quad (57)$$

where “NS,” “SO,” “SS,” and “SSS” denote the non-spinning, spin-orbit (linear-in-spin), spin-spin (quadratic-in-spin), and spin-spin-spin (cubic-in-spin) contributions, respectively; the explicit expressions for  $E_{\text{NS}}$  are given in, e.g., Ref. [42] while those for  $E_{\text{SO}}$ ,  $E_{\text{SS}}$  and  $E_{\text{SSS}}$  are given in, e.g., Ref. [44] and [130], respectively (see

also Refs. [135] and references therein). In the parenthesis of the right-hand side of the above equation, we have factored out  $\nu$  and  $M$  where  $\nu$  shows the leading PN order of each term and  $M$  is related to the powers of the spins. We note that the complete binding energy is also available up to 4PN order both in the spinning sector [124] and the non-spinning sector [75, 108, 35, 85], the latter of which has very recently been obtained:

$$E_{\text{NS}}^{4\text{PN}} = \nu^8 \left[ -\frac{3969}{128} + \left\{ -\frac{123671}{5760} + \frac{9037}{1536}\pi^2 + \frac{896}{15}\gamma_E + \frac{448}{15}\ln(16\nu) \right\} \eta \right. \\ \left. + \left( -\frac{498449}{3456} + \frac{3157}{576}\pi^2 \right) \eta^2 + \frac{301}{1728}\eta^3 + \frac{77}{31104}\eta^4 \right]. \quad (58)$$

Similarly, the 3.5PN corrections to the Newtonian energy flux (29) emitted to the infinity is written as

$$F_\infty \equiv \frac{32}{5}\eta^2\nu^{10} \left\{ F_{\text{NS}} + \frac{\nu^3}{M^2}F_{\text{SO}} + \frac{\nu^4}{M^4}F_{\text{SS}} + \frac{\nu^7}{M^6}F_{\text{SSS}} + O(\nu^8) \right\}. \quad (59)$$

The explicit expressions for  $F_{\text{NS}}$  and  $F_{\text{SO}}$  are given in, e.g., Ref. [42] while that for  $F_{\text{SS}}$  and  $F_{\text{SSS}}$  given in, e.g., Ref. [44] and [130], respectively (see also Refs. [135] and references therein). Currently, the complete form of GW fluxes beyond 3.5PN order is missing (only relative  $O(\eta)$  piece is available up to 11PN order [86]), and its derivation is a frontier in the PN calculations.

When the coalescing binary has at least one BH component, there is a part of the GW flux that goes down to the BH horizon, due to absorption effects of the energy and angular-momentum GW fluxes across the BH horizon. Such horizon flux appear at 2.5PN order for spinning BHs [173] (but it is pushed to 4PN order for non-spinning BHs [156, 93]) relative to the leading Newtonian-order energy flux (29), and it is known up to relative 1.5PN order for arbitrary mass ratio [57] (i.e., 4PN order beyond leading order energy flux) as well as 11PN order for the linear in the mass-ratio part [86], beyond the leading-order fluxes. The horizon fluxes (absorbed by the BH labelled by  $a$ ) may have the following factorized from

$$F_{\text{H}}^a(t; m_a, \chi_a) = \Omega_{\text{tidal}}(\Omega_H - \Omega_{\text{tidal}}) C_v^a, \quad (60)$$

where

$$C_v^a \equiv -\frac{16}{5} \frac{m_a^4}{M^2} \eta^2 \left( 1 + \sqrt{1 - \chi_a^2} \right) \nu^{12} \{ 1 + O(\nu^2) + \dots \}. \quad (61)$$

Here,  $\Omega_{\text{tidal}} = O(\nu^3)$  and  $\Omega_H$  are the angular velocities of the tidal field (caused by a companion BH) and the BH horizon, respectively. The coefficient  $C_v^a$  denotes the remaining factor determining the horizon flux, and it is needed to next-to-leading (relative 1PN) order to achieve 3.5PN order precision.



### ***Balance equation for slowly evolving black holes***

The most important equation in the adiabatic approximation, analog to Eq. (31) in linearized theory, is the energy balance equation. In the case of BBHs, it is written as

$$\frac{dE}{dt} = -F_\infty - \sum_a F_H^a, \quad (62)$$

where the change rate of the center-of-mass binding energy  $E$  (related to conservative dynamics), is equated to the energy fluxes of the GW emission carried out to infinity  $F_\infty$  and down to the BH horizon  $F_H^a$  (related to dissipative dynamics). A key assumption made in Eq. (62) is that the BH masses  $m_a$  and BH spins  $S_a$  remain constant in the inspiral phase until the adiabatic approximation itself breaks down.

However, this assumption is violated by horizon absorption effects. Each BH can be slowly evolving at the same time by changing its mass and spin via horizon absorption, namely

$$\frac{dm_a}{dt} = F_H^a, \quad \frac{dS_a}{dt} = \frac{1}{\Omega_{\text{tidal}}} \frac{dm_a}{dt}. \quad (63)$$

The absorption-corrected energy balance equation up to 3.5PN order is schematically given by Ref. [106]

$$\left( \frac{\partial \mathcal{E}}{\partial t} \right)_{m,S} = -\mathcal{F}_{\text{eff}} \equiv -\mathcal{F}_\infty - \sum_a (1 - \Gamma_H^a) \mathcal{F}_H^a, \quad (64)$$

where the absorption-corrected binding energy  $\mathcal{E}$  and fluxes  $\mathcal{F}_{\infty,H}$  are defined by corresponding  $E$  and  $F_{\infty,H}$ , promoting the constant BH mass  $m_a$  and spin  $S_a$  to the slowly evolving mass  $m_a(t)$  and spin  $S_a(t)$ . The BH's growth factors  $\Gamma_H^a = O(v^2)$  account for the fact that the derivative on the left hand is now partial one.

### ***Accuracy of the post-Newtonian approximants***

At this point, we must be mindful of the accuracy of the PN approximations. Two possible approaches to this problem have been extensively investigated in the literature. The first approach is to directly compare the PN waveform against the exact waveform from full NR simulations, performed in, e.g., Ref. [172]. The second approach is to compare physical quantities computed, such as the GW energy fluxes and binding energy (as well as linear momentum) that can be computed at higher PN order than the waveforms themselves: the modern development on both approaches is nicely summarised by Le Tiec's review [120].

This subsection is an additional contribution to the latter, based on the recent comparison of the GW energy fluxes [165]. The general strategy is to rely on Black Hole Perturbation (BHP) theory (see, e.g., Refs. [143, 134, 167] for reviews as

well as Chapter 36 by Pound and Barry in this book) outlined by earlier work in Refs. [182, 184] in which very high PN order calculations can be achieved systematically by further expanding the PN series in the mass ratio  $q$  assumed to be small; see also “Black Hole Perturbation Toolkit” at <http://bhptoolkit.org/> and “Black Hole Perturbation Club” at <https://sites.google.com/view/bhpc1996/home> for further details of the BH perturbation theory.

Consider a small body moving along the quasi equatorial-circular orbit in the Kerr spacetime with the mass  $M$  (note that  $M$  is not the total mass in this subsection) and Kerr spin parameter  $a/M$ . Assuming a “small-mass-ratio” limit ( $q \rightarrow 0$ ), the 11PN GW energy flux radiated to the infinity at the leading order in  $q$  has been computed [86]:

$$F^{(N)} = \sum_{k=0}^N \sum_{p=0}^{\lfloor k/6 \rfloor} F^{(k,p)} \{\ln(v)\}^p v^k, \quad (65)$$

where  $p$  and  $k$  are integer numbers and  $N = 22$ , and the leading order has been normalized to unity:  $F^{(0,0)} = 1$ .

The PN coefficients  $F^{(k,p)}$  are approximately fitted by a linear function with respect to  $k$  in the log-linear plot. As a specific example, the PN coefficient  $F^{(k,0)}$  versus  $k$  in the cases of the Kerr spin parameters of  $a/M = 0.99$  (for the retrograde orbit), 0, and 0.99 (for the prograde orbit) is displayed in Fig. 2. The inverted (blue) triangles, (black) circles, and (red) triangles denote  $F^{(k,0)}$  in the three cases, respectively. The dashed lines are the fitting lines for each case, and we find that  $F^{(k,0)}$  ( $k = 0, \dots, 22$ ) are fitted as  $(2.00014)^k$  for  $a/M = 0.99$  (retrograde),  $(1.94120)^k$  for  $a/M = 0.0$ , and  $(1.83690)^k$  for  $a/M = 0.99$  (prograde). These fittings suggest that the approximate radius of convergence in terms of the velocity parameter  $v$  is expected to be

$$\begin{aligned} v_{\text{conv}}(a/M = 0.99) &\sim 0.499965 \text{ (retrograde);} \\ v_{\text{conv}}(a/M = 0.00) &\sim 0.515145; \\ v_{\text{conv}}(a/M = 0.99) &\sim 0.544395 \text{ (prograde).} \end{aligned} \quad (66)$$

These values should be compared with the frequency at the innermost stable circular orbit (ISCO) because the quasicircular inspiral of a small body lasts until the orbital separation shrinks to the ISCO radius  $r_{\text{ISCO}}$  (in the Boyer-Lindquist coordinate). The ISCO radius in the equatorial plane of the Kerr spacetime is given by [33]

$$r_{\text{ISCO}} = M \left[ 3 + Z_2 \mp \{(3 - Z_1)(3 + Z_1 + 2Z_2)\}^{1/2} \right], \quad (67)$$

where  $Z_1 \equiv 1 + (1 - \chi^2)^{1/3} \{(1 + \chi)^{1/3} + (1 - \chi)^{1/3}\}$  and  $Z_2 \equiv (3\chi^2 + Z_1^2)^{1/2}$ . Here, the upper/lower sign refers to prograde/retrograde orbits. In Table 1, we summarize the ISCO radius ( $r_{\text{ISCO}}/M$ ), ISCO frequency ( $M\Omega_{\text{ISCO}} = \{(r_{\text{ISCO}}/M)^{3/2} + \chi\}^{-1}$ ) and the frequency parameter at ISCO ( $v_{\text{ISCO}} \equiv (M\Omega_{\text{ISCO}})^{1/3}$ ) for the representative Kerr spin parameters. Comparing the values of  $v_{\text{conv}}$  (66) and  $v_{\text{ISCO}}$  in Table 1, we expect that the PN series to the GW energy fluxes would work well up to ISCO for most of the retrograde orbits, but not for the prograde orbit with the high BH spin.

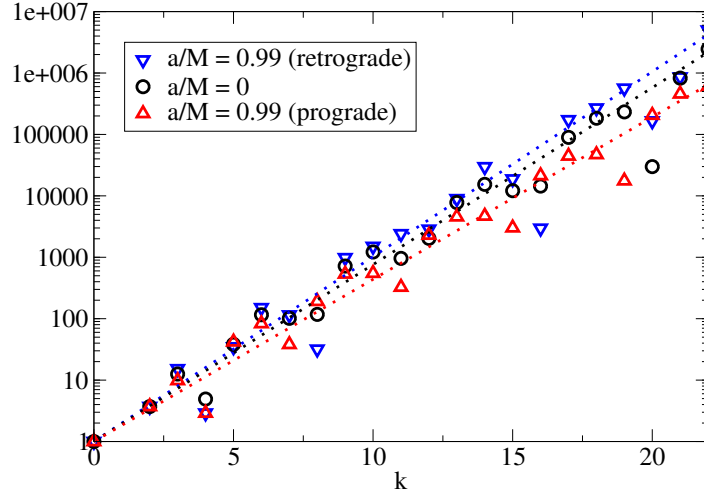


**Fig. 2** The inverted (blue) triangles, (black) circles, and (red) triangles denote  $F^{(k,0)}$  in Eq. (65) for the Kerr spin parameter  $a/M = 0.99$  (retrograde orbit), 0, and 0.99 (prograde orbit), respectively. The dashed lines are the fitting and show  $(2.00014)^k$  for  $a/M = 0.99$  (retrograde orbit),  $(1.94120)^k$  for  $a/M = 0$ , and  $(1.83690)^k$  for  $a/M = 0.99$  (prograde orbit).

**Table 1** The ISCO radius ( $r_{\text{ISCO}}/M$ ), ISCO frequency ( $M\Omega_{\text{ISCO}}$ ) and the frequency parameter a ISCO ( $v_{\text{ISCO}}$ ) for the representative Kerr spin parameters ( $a/M$ ); compare them against the values of the approximate radius of convergence  $v_{\text{conv}}$  in Eq. (66).

$a/M$	$r_{\text{ISCO}}/M$	$M\Omega_{\text{ISCO}}$	$v_{\text{ISCO}}$
1.0 (retrograde)	9.000000000	0.03571428571	0.3293168780
0.9 (retrograde)	8.717352279	0.03754018063	0.3348359801
0.5 (retrograde)	7.554584713	0.04702732522	0.3609525320
0.0	6.000000000	0.06804138173	0.4082482904
0.5 (prograde)	4.233002531	0.1085883589	0.4770835292
0.9 (prograde)	2.320883043	0.2254417086	0.6086179484
1.0 (prograde)	1.000000000	0.5000000000	0.7937005260

## Time- and Frequency-Domain Inspiral Templates

In this section we shall construct PN GW templates for the early adiabatic inspiral of spinning, nonprecessing BBHs, including the secular evolution of BH mass and spin. Our main goal is to obtain the phase function  $\phi(t)$  (53) to 3.5PN order, making use of the (BH-absorption corrected) PN binding energy (57), PN energy fluxes (59) and (60), and the generalized balance laws for the slowly evolving BHs (64) introduced in the previous section. The obtained phase in this way are called Taylor PN approximants [72, 73, 54]. For time-domain templates, we will present TaylorT1, TaylorT2, TaylorT3, TaylorT4 and TaylorT5 approximants. For the frequency-domain templates, we will show TaylorF1 and TaylorF2 approx-

imants. These Taylor approximants are formally equivalent up to the 3.5PN order, but the uncontrolled (higher-order) PN order terms are truncated differently.

Throughout the rest of this section, the labels “NS”, “SO”, “SS” and “SSS” denote the spinning, point-particle’s contributions, namely, without BH absorption of non-spinning, spin-orbit (linear-in-spin), spin-spin (quadratic-in-spin), and spin-spin-spin (cubic-in-spin) terms to the phase, while all the BH-absorption corrections are labelled by “Flux, 5” (from LO (2.5PN) horizon flux), “Flux, 7” (from NLO (3.5PN) horizon flux), and “BH, 7” (from slowly evolving, BH mass and spin). The explicit expressions for the point-particle contributions, not including absorption effect, are implemented in LALSimulation [126] (see also Ref. [54]) as “Module LALSimInspiralTaylorXX.c” at [https://lscsoft.docs.ligo.org/lalsuite/lalsimulation/group\\_\\_\\_l\\_a\\_l\\_sim\\_inspiral\\_taylor\\_x\\_x\\_c.html](https://lscsoft.docs.ligo.org/lalsuite/lalsimulation/group___l_a_l_sim_inspiral_taylor_x_x_c.html), while all the BH-absorption contributions are listed in Ref. [106].

Before proceeding, we note that our construction in this section is not complete. The frequency evolution due to changes in the BH’s mass and spin are constrained by (adiabatically invariant) “first-laws” of compact binary mechanics [122, 43, 87], which will be disregarded here; accounting for the first-law effect will await future work. See the recent work by Hughes [104] for details.

### *Taylor time domain approximants*

Using the balance equations (64), the evolution equations of the phase  $\phi(t)$  are [106]

$$\frac{d\phi}{dt} = \Omega = \frac{v^3}{M(v)}, \quad (68)$$

$$\frac{dv}{dt} = -\frac{\mathcal{F}_{\text{eff}}(v)}{(\partial\mathcal{E}/\partial v)_{M,S}}; \quad (69)$$

note that  $M(v)$  is a slowly evolving total BH mass, and  $\mathcal{E}$  and  $\mathcal{F}_{\text{eff}}$  are the absorption-corrected binding energy and (effective) fluxes. The different Taylor approximants integrate this system of ordinary differential equations differently. In each cases, the time-domain waveforms (in the restricted PN approximation) are obtained by inserting the resulting phase into, e.g., the leading-order GW polarizations  $h_{+, \times}$  (50), or the dominant  $(\ell, m) = (2, 2)$  mode  $h_{22}$  (55).

In the spinning, point-particle case (without BH absorption), these Taylor families of time-domain waveforms are implemented as “Module LALSimInspiralTaylorXX.c” at [https://lscsoft.docs.ligo.org/lalsuite/lalsimulation/group\\_\\_\\_l\\_a\\_l\\_sim\\_inspiral\\_taylor\\_x\\_x\\_c.html](https://lscsoft.docs.ligo.org/lalsuite/lalsimulation/group___l_a_l_sim_inspiral_taylor_x_x_c.html) in LALSimulation; the equations for the point-particle binaries are recovered by simply replacing  $\mathcal{E}$  and  $\mathcal{F}_{\text{eff}}$  with a “standard” expressions of  $E$  (57) and  $F_{\infty}$  (59) as well as the constant total mass  $M$  [126, 54].

### TaylorT1

The TaylorT1 phase,  $\phi^{\text{T1}}(t)$  is obtained by solving the system of two ordinary differential equations represented by Eqs. (68) and (69) with respect to time  $t$ . One may use  $v^{\text{T1}}(t)$  to calculate the GW amplitude.

### TaylorT4

Based on Ref. [51], first Taylor expands the ratio in the right-hand side of Eq. (69) and then truncate at appropriate PN order before integrating:

$$\frac{dv^{\text{T4}}}{dt} = \frac{dv_{\infty}^{\text{T4}}}{dt} + \frac{dv_{\text{H}}^{\text{T4}}}{dt}, \quad (70)$$

where  $dv_{\infty}^{\text{T4}}/dt$  describes the spinning point-particle contribution while  $dv_{\text{H}}^{\text{T4}}/dt$  accounts for the BH-absorption correction. Their formal PN structures are

$$\frac{dv_{\infty}^{\text{T4}}}{dt} = \frac{32}{5} \frac{\eta}{M} v^9 \{ \dot{v}_{\text{NS}}^{\text{T4}} + v^3 \dot{v}_{\text{SO}}^{\text{T4}} + v^4 \dot{v}_{\text{SS}}^{\text{T4}} + v^7 \dot{v}_{\text{SSS}}^{\text{T4}} + O(v^8) \}, \quad (71)$$

and

$$\frac{dv_{\text{H}}^{\text{T4}}}{dt} = \frac{32}{5} \frac{\eta}{M} v^{14} \{ \dot{v}_{\text{Flux},5}^{\text{T4}} + v^2 (\dot{v}_{\text{Flux},7}^{\text{T4}} + \eta \dot{v}_{\text{BH},7}^{\text{T4}}) + O(v^3) \}. \quad (72)$$

One then integrates two ordinary differential equations (68) and (70) at the same time. The resulting solutions  $v^{\text{T4}}(t)$  and  $\phi^{\text{T4}}(t)$  are TaylorT4 approximants. We note that among Taylor-based approximants, this waveform in the case of non-spinning quasicircular orbits, is the one that agrees more with NR waveforms for moderate values of the mass ratio  $0.5 \lesssim q \leq 1$  [46].

### TaylorT2

We rewrite Eqs. (68) and (69) as

$$\frac{d\phi}{dv} = \frac{v^3}{M(v)} \frac{dt}{dv}, \quad \frac{dt}{dv} = -\frac{(\partial \mathcal{E} / \partial v)_{M,S}}{\mathcal{F}_{\text{eff}}(v)}. \quad (73)$$

One can then analytically integrate this system with respect to  $v$  after re-expanding the right-hand sides of these expressions in PN series. The resulting solutions are TaylorT2 phase  $\phi^{\text{T2}}(v)$  and time  $t^{\text{T2}}(v)$ . We express them as

$$\phi^{\text{T2}}(v) = \phi_{\text{ref}}^{\text{T2}} + \phi_{\infty}^{\text{T2}}(v) + \phi_{\text{H}}^{\text{T2}}(v), \quad t^{\text{T2}}(v) = t_{\text{ref}}^{\text{T2}} + t_{\infty}^{\text{T2}}(v) + t_{\text{H}}^{\text{T2}}(v), \quad (74)$$

where  $\phi_{\text{ref}}^{\text{T2}}$  and  $t_{\text{ref}}^{\text{T2}}$  denote the reference phase and time as integration constants. The spinning point-particle contributions give rise to

$$\begin{aligned}\phi_{\infty}^{\text{T2}} &= -\frac{1}{32\eta v^5} \{ \phi_{\text{NS}}^{\text{T2}} + v^3 \phi_{\text{SO}}^{\text{T2}} + v^4 \phi_{\text{SS}}^{\text{T2}} + v^7 \phi_{\text{SSS}}^{\text{T2}} + O(v^8) \}, \\ t_{\infty}^{\text{T2}} &= -\frac{5M}{256\eta v^8} \{ t_{\text{NS}}^{\text{T2}} + v^3 t_{\text{SO}}^{\text{T2}} + v^4 t_{\text{SS}}^{\text{T2}} + v^7 t_{\text{SSS}}^{\text{T2}} + O(v^8) \},\end{aligned}\quad (75)$$

while the BH-absorption corrections are

$$\begin{aligned}\phi_{\text{H}}^{\text{T2}} &= -\frac{1}{32\eta} \{ \ln(v) \phi_{\text{Flux},5}^{\text{T2}} + v^2 (\phi_{\text{Flux},7}^{\text{T2}} + \eta \phi_{\text{BH},7}^{\text{T2}}) + O(v^3) \}, \\ t_{\text{H}}^{\text{T2}} &= -\frac{5M}{256\eta v^3} \{ t_{\text{Flux},5}^{\text{T2}} + v^2 (t_{\text{Flux},7}^{\text{T2}} + \eta t_{\text{BH},7}^{\text{T2}}) + O(v^3) \},\end{aligned}\quad (76)$$

Here, all the terms are expressed in the PN series (analytically). TaylorT2 approximants are useful to understand the contributions of each term because the total expressions are summed up.

### TaylorT3

Inverting the PN series  $t(v)$  (like TaylorT2 time  $t^{\text{T2}}(v)$ ) to obtain  $v(t)$  analytically, we can re-express the TaylorT2 phase with respect to  $t$  via the relation  $\phi(t) \equiv \phi(v(t))$ . These are the TaylorT3 approximants. With the dimensionless time variable ( $t_{\text{ref}}^{\text{T2}}$  is analogue to the coalescence  $t_c$  introduced in Eq. (35)),

$$\theta \equiv \left\{ \frac{\eta}{5M} (t_{\text{ref}}^{\text{T2}} - t) \right\}^{-1/8}, \quad (77)$$

one obtains

$$\phi^{\text{T3}}(\theta) = \phi_{\text{ref}}^{\text{T3}} + \phi_{\infty}^{\text{T3}}(\theta) + \phi_{\text{H}}^{\text{T3}}(\theta), \quad F^{\text{T3}}(\theta) = F_{\infty}^{\text{T3}}(\theta) + F_{\text{H}}^{\text{T3}}(\theta), \quad (78)$$

where  $F \equiv (2d\phi/dt)/(2\pi) = v^3/(\pi m)$  is the GW frequency of the dominant  $(\ell, m) = (2, 2)$  GW mode, and the meaning of the labels “ $\infty$ ” and “H” are the same as Eq. (74). Their formal PN structures are

$$\begin{aligned}\phi_{\infty}^{\text{T3}} &= -\frac{1}{\eta \theta^5} \{ \phi_{\text{NS}}^{\text{T3}} + \theta^3 \phi_{\text{SO}}^{\text{T3}} + \theta^4 \phi_{\text{SS}}^{\text{T3}} + \theta^7 \phi_{\text{SSS}}^{\text{T3}} + O(\theta^8) \}, \\ F_{\infty}^{\text{T3}} &= \frac{\theta^3}{8\pi M} \{ F_{\text{NS}}^{\text{T3}} + \theta^3 F_{\text{SO}}^{\text{T3}} + \theta^4 F_{\text{SS}}^{\text{T3}} + \theta^7 F_{\text{SSS}}^{\text{T3}} + O(\theta^8) \},\end{aligned}\quad (79)$$

and

$$\phi_{\text{H}}^{\text{T3}} = -\frac{1}{\eta} \{ \ln(\theta) \phi_{\text{Flux},5}^{\text{T3}} + \theta^2 (\phi_{\text{Flux},7}^{\text{T3}} + \eta \phi_{\text{BH},7}^{\text{T3}}) + O(\theta^3) \},$$

$$F_H^{\text{T3}} = \frac{\theta^8}{8\pi M} \{F_{\text{Flux},5}^{\text{T3}} + \theta^2 (F_{\text{Flux},7}^{\text{T3}} + \eta F_{\text{BH},7}^{\text{T3}}) + O(\theta^3)\}. \quad (80)$$

The TaylorT3 waveform is useful when plotting inspiral GW waveforms in the time domain because the GW phase (by using  $\phi^{\text{T3}}$ ) and amplitude (by using  $F^{\text{T3}}$ ) are written with respect to  $t$  directly.

### TaylorT5

A variant of the TaylorT2 construction has been adopted to define the TaylorT5 approximants in Ref. [21]. It consists in Taylor expanding in  $v$  the right-hand side of the second equation of Eq. (73), the one for  $dt/dv$ , truncating it to the appropriate order, then taking its inverse, and integrating it to obtain  $v(t)$ .

The phasing is then obtained by substituting  $v(t)$  inside the analytical expression of  $\phi(v)$  and direct integration of the Taylor expanded  $d\phi/dv$ .

### Taylor frequency-domain approximants

For an adiabatic BBH inspiral, the frequency-domain waveform is conveniently constructed using the stationary phase approximation (SPA), described in the subsection ‘‘Stationary phase approximation’’ (see also, e.g., Ref. [135] and references therein). In the case of the dominant  $(\ell, m) = (2, 2)$  GW modes  $h_{22}$ , for instance, we model the Fourier amplitude  $A(f)$  and the Fourier-domain phase  $\Psi(f)$  defined by

$$\tilde{h}_{22}(f) = A(f) e^{i(\Psi_{\text{SPA}}(f) - \pi/4)}, \quad \Psi_{\text{SPA}}(f) = 2\pi f t(f) - \Psi(f). \quad (81)$$

The SPA Fourier amplitude with evolving reduced mass  $\mu(v)$  is

$$A(f) \simeq \frac{8\mu(v)}{r} \sqrt{\frac{\pi}{5}} v^2 \left( \frac{3v^2}{\pi M} \frac{dv}{dt} \right)^{-1/2} \Big|_{v=v_f}, \quad (82)$$

where  $v_f \equiv (\pi M f)^{1/3}$  is a dimensionless Fourier parameter (normalised by the initial values of the total mass  $M = M_I$ ) and  $dv/dt$  is given in Eq. (69). At the same time, the SPA Fourier-domain phase is obtained by solving the set of ordinary differential equations:

$$\frac{d\Psi_{\text{SPA}}}{df} - 2\pi t = 0, \quad \frac{dt}{df} + \frac{\pi M}{3v^2} \frac{(\partial \mathcal{E} / \partial v)_{m,S}}{\mathcal{F}_{\text{eff}}(v)} = 0. \quad (83)$$

Again,  $\mathcal{E}$  and  $\mathcal{F}_{\text{eff}}$  are the absorption-corrected binding energy and (effective) fluxes: recall Eq. (64). The different Taylor approximants integrate Eqs. (82) and (83) differently.

In the spinning, nonprecessing point-particle case (without BH absorption) TaylorF2 waveforms are implemented as “Module LALSimInspiralTaylorF2.c” at [https://lscsoft.docs.ligo.org/lalsuite/lalsimulation/group\\_\\_l\\_a\\_l\\_sim\\_inspiral\\_taylor\\_x\\_x\\_\\_c.html](https://lscsoft.docs.ligo.org/lalsuite/lalsimulation/group__l_a_l_sim_inspiral_taylor_x_x__c.html) in LALSimulation; the equations for the point-particle binaries are recovered by replacing  $\mathcal{E}$  and  $\mathcal{F}_{\text{eff}}$  in Eq. (83) with  $E$  (57),  $F_\infty$  (59) and the constant total mass  $M$  [126, 54].

### TaylorF1

The direct numerical integration of Eqs. (82) and (83) gives the TaylorF1 amplitude  $A^{\text{F1}}(f)$  and the TaylorF1 phase  $\Psi_{\text{SPA}}^{\text{F1}}(f)$ , respectively. One may use the TaylorT4  $dv^{\text{T4}}/dt$  (70) as input PN expression for  $dv/dt$  when solving Eq. (82).

### TaylorF2

Drawing an analogy with TaylorT2, we re-expand the right-hand sides of Eqs. (82) and (83) in the PN series and analytically integrate them with respect to  $f$ . The TaylorF2 phase is then given by

$$\Psi_{\text{SPA}}^{\text{F2}}(f) = 2\pi f t_c - \Psi_c + \Psi_\infty^{\text{F2}}(f) + \Psi_{\text{H}}^{\text{F2}}(f), \quad (84)$$

where  $t_c$  and  $\Phi_c$  are constants that we can choose arbitrarily. The spinning point-particle contribution is

$$\Psi_\infty^{\text{F2}}(f) = \frac{3}{128\eta v^5} \{ \Psi_{\text{NS}}^{\text{F2}} + v_f^3 \Psi_{\text{SO}}^{\text{F2}} + v_f^4 \Psi_{\text{SS}}^{\text{F2}} + v_f^7 \Psi_{\text{SSS}}^{\text{F2}} + O(v_f^8) \}, \quad (85)$$

while the BH-absorption contributions are

$$\Psi_{\text{H}}^{\text{F2}}(f) = \frac{3}{128\eta} \left[ \left\{ 1 + 3 \ln \left( \frac{v_f}{v_{\text{reg}}} \right) \right\} \Psi_{\text{Flux},5}^{\text{F2}} + v_f^2 (\Psi_{\text{Flux},7}^{\text{F2}} + \eta \Psi_{\text{BH},7}^{\text{F2}}) + O(v_f^3) \right], \quad (86)$$

where the constant  $v_{\text{reg}}$  can be chosen arbitrary.

The TaylorF2 amplitude  $A^{\text{F2}}(f)$  is given by inserting TaylorT4  $dv^{\text{T4}}/dt$  (70) into Eq. (82) and re-expanding it in the PN series and truncate at 3.5PN order. The most commonly used TaylorT2 amplitude is, however, in the restricted PN approximation given by

$$A^{\text{F2}}(f) \simeq \frac{\mathcal{M}^{5/6}}{r} \sqrt{\frac{2}{3\pi^{1/3}}} f^{-7/6} \{1 + O(v^2)\}. \quad (87)$$

It is worth noting that the spin effects at the leading 1.5PN order (i.e., the leading spin-orbit term) in the SPA amplitude and phase are encoded in a single spin parameter, the effective aligned spin [65],  $\chi_{\text{eff}} \equiv (m_1 \chi_1 + m_2 \chi_2)/M$  or the reduced spin parameter [21]



$$\chi_{\text{PN}} \equiv \chi_{\text{eff}} - \frac{38\eta}{113}(\chi_1 + \chi_2), \quad (88)$$

used for waveform calibration against NR waveform in inspiral-merger-ringdown waveforms which we will introduce in the next section.

### ***Beyond spinning, nonprecessing Binary Black Hole cases***

Until this subsection, we have confined our attention to the simplest adiabatic inspiral of a spinning, nonprecessing BBH without orbital eccentricity. The leap from this narrow case to a generic case of binary configurations – in particular, one of the component compact objects is a NS rather than a BH – comes with a number of consequences.

Below we briefly review some of the key elements when constructing PN templates for generic inspirals; the inclusion of merger and ringdown phase with completely generic waveform models will be summarized in the next section.

*Eccentricity.*— The radiative loss of the orbital energy and angular momentum to GWs circularizes the orbits of inspirals. The averaged rates of change of orbital eccentricity  $e(\leq 1)$  due to the radiative losses in the adiabatic approximation are estimated as (see, e.g., Chapter 12 of Poisson and Will [157], and Ref. [152])

$$\frac{de}{dt} = -\frac{304}{15}\eta\frac{e}{a}\left(\frac{M}{a}\right)^3(1-e^2)^{-5/2}\left(1+\frac{121}{304}e^2\right), \quad (89)$$

where  $a$  is the semi-major axis of the ellipse (not the Kerr spin parameter here) and we assume Newtonian elliptic orbits for simplicity. That is, the eccentricity always decreases when the orbit shrinks as approaching the merger phase. In fact, assume a small eccentricity limit  $e \ll 1$ , Eq. (89), can be integrated (with the help of  $da/dt$  etc.) to give  $e \simeq e_{\text{ini}}(a/a_{\text{ini}})^{19/12}$ , where  $a_{\text{ini}}$  and  $e_{\text{ini}}$  are initial values. We clearly see that the orbit is circularised quite fast toward the late inspiral phase.

Nevertheless, there is emerging need for GW models for the quasicentric inspirals because it will be an important source for the next-generation GW detectors both on the ground (e.g., KAGRA+ [133], Voyager (<https://dcc.ligo.org/LIGO-G1602258/public>), Einstein Telescope [101], Cosmic Explorer [163], etc) and in the space (e.g., LISA [29], (B-)DECIGO [110], TianQin [132], etc), which have wider sensitivity band for the early inspiral phase; see also Chapter 3 by Gair et al. and Chapter 7 by Lueck et al. in this book. There is an ongoing program of development on the waveforms for the quasicentric binaries. A theoretical GW waveform for non-spinning eccentric binaries has been developed in Refs. [103, 137, 174, 179, 178] with the quasi-Keplerian formalism (see also Chapter 10 of Ref. [42] and references therein). This waveform is valid for the small initial orbital eccentricity, and its frequency-domain model is implemented in LALSImulation as TaylorF2Ecc at [https://lscsoft.docs.ligo.org/lalsuite/lalsimulation/group\\_\\_l\\_a\\_l\\_sim\\_inspiral\\_taylor\\_f2\\_ecc\\_c](https://lscsoft.docs.ligo.org/lalsuite/lalsimulation/group__l_a_l_sim_inspiral_taylor_f2_ecc_c).

[html](#) (see also EccentricTD/FD modules). However, a GW waveform that performs well even at large eccentricities requires further development. Recent efforts can be found in, e.g., Refs. [138, 136] and Chapter 33 by Loutrel in this book.

*Spin precession.*— In the nonprecessing system, the spins of the compact objects are (anti-)parallel to the orbital-angular momentum; the orbital plane of binary is fixed. If the spins are not aligned with the orbital angular momentum the spin-orbit and spin-spin effects lead to precession of the spins and orbital plane, while the total angular momentum is constant, modulo angular momentum loss via radiation. The precession timescale for the spinning binaries is

$$t_P = \frac{|\mathbf{S}_a|}{|d\mathbf{S}_a/dt|} \sim Mv^{-5}, \quad (90)$$

which is shorter than the radiation reaction timescale  $t_{RR}/M \propto v^{-8}$  given in Eq. (32), hence neglecting losses the orbital and spin angular momentum precess around the total angular momentum. Schematically, the (orbital-averaged) spin precession equations that govern the conservative evolution of spin vectors are (see, e.g., Chapter 9 of Poisson and Will [157] and Ref. [52] for the explicit expressions)

$$\frac{d\mathbf{S}_a}{dt} = \left( \boldsymbol{\Omega}_a^{\text{SO}} + \boldsymbol{\Omega}_a^{\text{SS}} \right) \times \mathbf{S}_a, \quad (91)$$

where  $\boldsymbol{\Omega}_a^{\text{SO,SS}}$  are spin-orbit and spin-spin pieces of the precessional angular velocity. The frequency  $\boldsymbol{\Omega}_a^{\text{SO}}$  describes the spin-orbit (geodetic) precession of the spin vectors while  $\boldsymbol{\Omega}_a^{\text{SS}}$  is responsible for the spin-spin (frame-dragging) precession of those spin vectors.

The precession determined by Eq. (91) then modulates the waveform, adding rich periodic structure, as the angle between the normal to the orbit and the line of sight also precesses. As a result, the GW mode  $(\ell, m) = (2, 2)$  is no longer guaranteed to be the “dominant” one; all the  $\ell = 2$  modes become relevant. These complications make the modeling of precessing waveform challenging, but they gain us access to more binary parameters that can be hard to measure in nonprecessing binaries, due to their degeneracies with other parameters that can be disentangled by observing the source’s plane from different angles during the very same inspiral.

For more recent effort to develop the precessing binary waveforms, see, e.g., a concise review by Hannam [95] (and references therein, also see [58]). Various spin precessing Taylor waveforms are implemented in LALsimulation and are found at [https://lscsoft.docs.ligo.org/lalsuite/lalsimulation/group\\_\\_l\\_a\\_l\\_sim\\_inspiral\\_spin\\_taylor\\_\\_c.html](https://lscsoft.docs.ligo.org/lalsuite/lalsimulation/group__l_a_l_sim_inspiral_spin_taylor__c.html).

*Matter effects.*— When one of binary components is not a BH, but a material body as NS, it can acquire a quadrupole moment induced by, e.g., the tidal field generated by its companion. It is particularly interesting since the deformation giving rise to the tidally induced quadrupole bears the imprint of the equation of state of the NS – i.e., the microscopic property of strongly interacted nuclear matter under extreme conditions of pressure and density.

The induced quadrupole moment of NSs is mainly characterised by two physical effects. The first one is due to (static) tides, as non-spinning NS of mass  $m_a$  and radius  $R_a^{\text{NS}} \ll R$  in a binary is subjected to a tidal field by the companion. In a Newtonian gravity (for simplicity), a tidally induced quadrupole moment is given by

$$Q_a^{\text{tidal}} \sim \lambda_a \frac{m_b}{R^3}, \quad (92)$$

where  $\lambda_a = k_a (R_a^{\text{NS}})^5$  is the (static) tidal deformability defined in terms of the dimensionless (gravitational) Love number  $k$  that depends on the NS's equation of state. A measurement of  $k_a$  or  $\lambda_a$  through the use of GW therefore provides unique insight into NS matter; we note that  $k_a = 0$  for a non-spinning, Schwarzschild BH (the tidally induced quadrupole moments of Schwarzschild BH vanish in the static case [41, 69, 115] and is proportional to the inducing field time derivatives, being a dissipative effect, giving rise to the horizon fluxes discussed in the previous section [154]). The GW astronomy on the NS tidal deformability is described in detail, e.g., by Chatziioannou [56]; see also Chapter 11 by Baiotti and Chapter 14 by Foucart in this book.

For non-spinning BNSs, the family of PN templates with tidal interactions is nicely summarised in, e.g., Ref. [145] and Chapter 4 by Dietrich et al. [78]. As an example, we briefly summarise the *Kyoto*'s phenomenological model by Kawaguchi et al. [109], which combines the PN tidal corrections with phenomenological terms obtained by fits to *Kyoto*'s high-precision NR waveforms. In this model, TaylorF2 (strain)  $\tilde{h}(f) = A(f) e^{i\Psi(f)}$  with the tidal contributions may take the split form of

$$A(f) = A_{\text{PP}}(f) + A_{\text{Tidal}}(f), \quad \Psi(f) = \Psi_{\text{PP}}(f) + \Psi_{\text{Tidal}}(f), \quad (93)$$

where ‘‘PP’’ and ‘‘tidal’’ are individual contributions from the non-spinning point particle and tidal interactions, respectively. The tidal terms  $A_{\text{Tidal}}(f)$  and  $\Psi_{\text{Tidal}}(f)$  are then given by (note that  $x \equiv v^2$ )

$$\begin{aligned} A_{\text{Tidal}}^{\text{Kyoto}} &= \sqrt{\frac{5\pi\eta}{24}} \frac{M^2}{r} \tilde{\Lambda} x^{-7/4} \times \left( -\frac{27}{16} x^5 - \frac{449}{64} x^6 - b x^r \right), \\ \Psi_{\text{Tidal}}^{\text{Kyoto}} &= \frac{3}{128\eta} \left\{ -\frac{39}{2} \tilde{\Lambda} \left( 1 + a \tilde{\Lambda}^{2/3} x^p \right) \right\} x^{5/2} \\ &\quad \times \left( 1 + \frac{3115}{1248} x - \pi x^{3/2} + \frac{28024205}{3302208} x^2 - \frac{4283}{1092} \pi x^{5/2} \right), \end{aligned} \quad (94)$$

with  $a = 12.55$ ,  $p = 4.240$ ,  $b = 4251$  and  $r = 7.890$ . Here,  $\tilde{\Lambda}$  is the combination of the individual (dimensionless) tidal deformability  $\Lambda_a \equiv \lambda_a/m_a^5$  defined by [82]

$$\tilde{\Lambda} = \frac{16}{13} \frac{(m_1 + 12m_2)m_1^4 \Lambda_1 + (m_2 + 12m_1)m_2^4 \Lambda_2}{M^5}. \quad (95)$$

This parameter characterises the leading-order (relative 5PN) tidal effects in the waveforms.

TaylorF2 with tidal effects was used to analyze the first BNS event, GW170817 [11], and it is implemented in LALSimulation as a part of “Module LALSimInspiralTaylorXX.c” at [https://lscsoft.docs.ligo.org/lalsuite/lalsimulation/group\\_\\_l\\_a\\_l\\_sim\\_inspiral\\_taylor\\_x\\_x\\_\\_c.html](https://lscsoft.docs.ligo.org/lalsuite/lalsimulation/group__l_a_l_sim_inspiral_taylor_x_x__c.html). For more improved analysis of GW170817 [4], a different model was used as a reference. In GWTC-1 [3], this is also used as a frequency-domain model for GW170817. For example, we will see the SEOBNRv4\_ROM\_NRTidal and IMRPhenomPv2\_NRTidal models in the next section.

The second effect that gives rise to the induced quadrupole moment is the rotation. The spinning motion deforms the NS by creating a distortion in its mass distribution, which also depends on the NS’s equation of state [118]. The resultant (relativistic) spin-induced quadrupole moment is given by [153]

$$Q_a^{\text{spin}} \simeq \alpha \chi_a^2 m_a^3, \quad (96)$$

where  $\alpha$  is the (dimensionless) spin deformability. Although the known NS has low spin in general ( $\chi_a \sim 0.2$  or less [11, 7]), in principle, the measurement of  $\alpha$  for highly spinning BNSs would provide another GW probe to NS matter [100]. We note that  $\alpha = 1$  for Kerr BHs, followed by its well-known “no-hair” property.

By likewise writing  $\Psi_{\text{Tidal}}$ , the correction to the TaylorF2 phase due to the NS’s quadrupole spin-deformation is given by [153, 117].

$$\Psi_{QM} = \frac{3}{128\eta} (-25\tilde{Q}) v^{-1} + O(v), \quad (97)$$

where  $\tilde{Q}$  is a certain combination of the individual spin-induced quadrupole deformation  $Q_a^{\text{spin}}$  and spins  $\chi_a$ , which characterise the leading-order (relative 2PN) effects in the waveform. It is implemented in LALSimulation within “Module LALSimInspiralSpinTaylor.c” ([https://lscsoft.docs.ligo.org/lalsuite/lalsimulation/group\\_\\_l\\_a\\_l\\_sim\\_inspiral\\_spin\\_taylor\\_c.html](https://lscsoft.docs.ligo.org/lalsuite/lalsimulation/group__l_a_l_sim_inspiral_spin_taylor_c.html)), and the quadrupole spin-deformation contribution to energy, flux, and phasing terms are coded in [https://lscsoft.docs.ligo.org/lalsuite/lalsimulation/\\_l\\_a\\_l\\_sim\\_inspiral\\_p\\_n\\_coefficients\\_8c.html](https://lscsoft.docs.ligo.org/lalsuite/lalsimulation/_l_a_l_sim_inspiral_p_n_coefficients_8c.html).

## Full Inspiral-Merger-Ringdown waveform models

In our discussion so far, we have focused exclusively on the GW waveforms from adiabatic inspirals within the PN approximation. However, this is just a part of GW signals from the coalescence of compact-object binaries that can be observed by LIGO, Virgo, and KAGRA.

As the separation of binary shrinks (by “chirping” the frequency  $\nu \rightarrow 1$ ), the binary dynamics moves on to the merger phase, and the PN calculations become more and more inaccurate; recall our discussion on the accuracy of the PN approximants. The modelling in the late inspiral phase should be modified to enhance the accuracy

of PN approximation. The transition frequency from inspiral to the merger phase is roughly estimated by the GW frequency at ISCO of Schwarzschild BH with the mass  $M_{\text{Sch}}$ :

$$f_{\text{ISCO}} \approx 73.28 \left( \frac{M_{\text{Sch}}}{60M_{\odot}} \right)^{-1} \text{ Hz} \approx 1570 \left( \frac{M_{\text{Sch}}}{2.8M_{\odot}} \right)^{-1} \text{ Hz}. \quad (98)$$

This is well in the sensitive frequency band of LIGO, Virgo and KAGRA.

Furthermore, the ringdown phase followed by the merger phase has the typical GW frequency at [39]

$$f_{\text{Ring}} = 538.4 \left( \frac{M_{\text{Rem}}}{60M_{\odot}} \right)^{-1} \{ 1.5251 - 1.1568(1 - \alpha_{\text{Rem}})^{0.1292} \} \text{ Hz}, \quad (99)$$

where  $M_{\text{Rem}}$  and  $\alpha_{\text{Rem}}$  are the mass and non-dimensional spin of the remnant Kerr BH after merger. The above expression gives 198.3 Hz for  $M_{\text{Rem}} = 60M_{\odot}$  and  $\alpha_{\text{Rem}} = 0$ . This ringdown frequency, especially for BBHs, is again well in the sensitivity band of the Advanced LIGO, Virgo, and KAGRA. Therefore, it is indispensable to have a “full” waveform, including the merger and ringdown phases in addition to the PN model for the inspiral phase, in order to maximise our ability to GW data analysis.

The goal of this section is to briefly survey such a full, inspiral-merger-ringdown (IMR) waveform actually implemented and used for the GW data analysis of the first, second and third observing runs (O1, O2, and O3) of Advanced LIGO and Virgo; more details are covered in Chapter 35 by McWilliams in this book, and the IMR waveform models used in the up-to-date GWTC-2 [18] are summarised in Table III of that paper. There are two main families of the IMR waveform; the effective-one-body (EOB) approach (in the time-domain), and the “phenomenological” (IMRPhenom) models (in the frequency-domain). All the details of these two methods in LALsimulation can be found at [https://lscsoft.docs.ligo.org/lalsuite/lalsimulation/group\\_\\_l\\_a\\_l\\_sim\\_i\\_m\\_r\\_h.html](https://lscsoft.docs.ligo.org/lalsuite/lalsimulation/group__l_a_l_sim_i_m_r_h.html). We should note, however, that these methods in LALsimulation ignore any of contributions of BH absorption discussed in the previous section.

### ***Effective-one-body (EOB) approach***

An effective-one-body (EOB) approach [49, 50] is an analytical framework to cover the full range of the inspiral, merger, and ringdown phases, making use of a variety of analytical approximation methods, such as the PN theory and the Black Hole Perturbation (BHP) theory, and NR data as calibrations. A brief review of the EOB approach is given in Refs. [66, 67]; see also, e.g., Refs. [68, 30] (and reference therein) for latest developments.

The starting point of the EOB approach is to precisely describe the orbital dynamics of binaries (as a source of GW waveform). First, one conveniently maps the real two-body PN Hamiltonian (for their relative motion) to an “effective” test-particle Hamiltonian  $H^{\text{eff}}$  of non-geodesic motion in a fictitious effective spacetime, so as to construct the so-named EOB (or “improved real”) Hamiltonian:

$$H^{\text{EOB}} \equiv M \sqrt{1 + 2\eta \left( \frac{H^{\text{eff}}}{\mu} - 1 \right)}. \quad (100)$$

In general,  $H^{\text{EOB}}$  improves the convergence of PN series of the original PN Hamiltonian. Second, the radiation reaction to the system, which is another piece to describe the radiative dynamics of binaries, is prepared from, e.g., the PN and BHP results of the GW fluxes with a resummation such as a Padé approximation or the factorised resummation [70, 71]. Third, one introduces some adjustable free parameters to the Hamiltonian and fluxes and calibrates them against the results of NR simulations (and that of the BHP and self-force theory [32] in the small-mass-ratio limit,  $q \rightarrow 0$ ). In particular, the EOB models calibrated to NR simulations are dubbed as “EOBNR.”

The next step is to construct GW waveforms from the obtained EOB orbital dynamics. The inspiral-plus-plunge GW waveform  $h_{\text{insplunge}}$  is derived from the orbital motion, based on the improved resummation of PN (multipolar) inspiral waveforms [74, 149], including non-quasicircular effects [70, 71]. This waveform is connected smoothly to a ringdown GW waveform  $h_{\text{ringdown}}$  which consists of several quasinormal modes of the remnant BH after merger, around a matching time  $t_{\text{match}}$  (see Ref. [40] and references therein for the ringdown phase). The full GW waveform is then schematically written as [71]

$$h_{\text{EOB}}(t) = \theta(t_{\text{match}} - t) h_{\text{insplunge}}(t) + \theta(t - t_{\text{match}}) h_{\text{ringdown}}(t), \quad (101)$$

where  $\theta(t)$  is the Heaviside-step function.

In Ref. [53], the EOBNRv1 model was proposed for non-spinning BBHs. This was calibrated to NR simulations with mass ratios,  $m_1/m_2 = 1, 3/2, 2,$  and 4. In Ref. [148], the EOBNRv2 model was proposed for the same non-spinning case. This was also calibrated to NR simulations with mass ratios,  $m_1/m_2 = 1, 2, 3, 4$  and 6. The above two GW waveform approximants include not only the dominant  $(\ell, |m|) = (2, 2)$  modes, but also some subdominant harmonic modes; see also Section II-a in Ref. [2]. In the classical GW data analysis of the LIGO fifth science run (S5) [2], these two EOBNR models were used as an IMR theoretical template, and the EOBNRv2 model is available at [https://lscsoft.docs.ligo.org/lalsuite/lalsimulation/group\\_\\_l\\_a\\_l\\_sim\\_i\\_m\\_r\\_e\\_o\\_b\\_n\\_rv2\\_\\_c.html](https://lscsoft.docs.ligo.org/lalsuite/lalsimulation/group__l_a_l_sim_i_m_r_e_o_b_n_rv2__c.html); note, however, that EOBNRv1/v2 models have been superseded by more recent developments (such as SEOBNR family below) and they are no longer used in the modern LAL simulation.

### SEOBNR family

*SEOBNRv1/v2*.— In Ref. [175, 176] (and references therein), EOB models have been presented for spinning, nonprecessing BBHs (the first character, “S” in SEOBNR denotes spin). The SEOBNRv1 and SEOBNRv2 models are available at [https://lscsoft.docs.ligo.org/lalsuite/lalsimulation/group\\_\\_l\\_a\\_l\\_sim\\_i\\_m\\_r\\_spin\\_aligned\\_e\\_o\\_b\\_\\_c.html](https://lscsoft.docs.ligo.org/lalsuite/lalsimulation/group__l_a_l_sim_i_m_r_spin_aligned_e_o_b__c.html). The parameters of the first BBH event, GW150914 [8] was evaluated by the SEOBNRv2 model. This was also used in the detailed study on the properties of GW150914 [9]. SEOBNRv2\_ROM\_DoubleSpin [81] which speeds up the waveform generation with reduced-order modelling (ROM) [162] was also used.

*SEOBNRv3*.— In Ref. [150], the SEOBNRv3 model has been presented as a fully precessing waveform model for BBH coalescence. The SEOBNRv3 model is available at [https://lscsoft.docs.ligo.org/lalsuite/lalsimulation/\\_l\\_a\\_l\\_sim\\_i\\_m\\_r\\_spin\\_prec\\_e\\_o\\_b\\_8c.html](https://lscsoft.docs.ligo.org/lalsuite/lalsimulation/_l_a_l_sim_i_m_r_spin_prec_e_o_b_8c.html). This SEOBNRv3 model was used in the detailed study on the properties of GW150914 [9]. Also, in GWTC-1 [3], the SEOBNRv3 model was used to analyse generic two-spin precession dynamics.

*SEOBNRv4/v4HM*.— For spinning, nonprecessing BBHs, the SEOBNRv4 model [45] is an improvement of the SEOBNRv2 model with calibration to 141 NR waveforms including the spin effects. As a further improved version of the SEOBNRv4 model with higher harmonics, the SEOBNRv4HM model is presented (HM standing for “Higher Modes”) [62]. The SEOBNRv4 and SEOBNRv4HM models are available at [https://lscsoft.docs.ligo.org/lalsuite/lalsimulation/group\\_\\_l\\_a\\_l\\_sim\\_i\\_m\\_r\\_spin\\_aligned\\_e\\_o\\_b\\_\\_c.html](https://lscsoft.docs.ligo.org/lalsuite/lalsimulation/group__l_a_l_sim_i_m_r_spin_aligned_e_o_b__c.html) where all aligned spin, i.e., nonprecessing models, are summarized.

For the analysis of GW170817 in Ref. [4] with the help of the NRTidal model for the tidal effects (a hybrid model mainly based on the PN tidal phase corrections up to the 7.5PN order and the calibration against the high-precision NR data) [79, 76, 77]

$$\text{SEOBNRv4\_ROM\_NRTidal} = \text{SEOBNRv4\_ROM} + \text{NRTidal}$$

was used as a signal model of BNS mergers.

In GWTC-1 [3], this was also used as a frequency-domain model for GW170817. In the analysis of GW190814 [15], there was no measurable tidal signature although the SEOBNRv4\_ROM\_NRTidalv2\_NSBH model with phenomenological tidal effects and the NS’s tidal disruption was applied. The SEOBNRv4T model [102] which gives a time-domain waveform with analytical dynamic tide effects has been also used in GWTC-1 [3] for GW170817.

*SEOBNRv4P/v4PHM*.— The EOBNR model with higher multipoles for precessing binaries (see Refs. [62, 147] and references therein) was used for GW190412 [13]. Also, this model has been used for GW190814 [15], GW190521 [14], and GWTC-2 [18] as a BBH waveform model. The precessing model SEOBNRv4PHM also includes its restriction to the dominant GW modes, SEOBNRv4P.

## TEOBResumS

The TEOBResumS has been the first to implement a tidal description up to merger verified with NR simulations [37, 25, 36, 142], and it is the only model that implements a binary NS post-merger completion [48] so to give a complete description of the signal emitted by binary NSs. Note that especially the method of calibration against NR simulations is different from the above EOBNR family; see Section VI of Ref. [142]. Spin interactions in the BNS waveforms are included at next-next-leading order [139] and include precession effects [26]. The BBH sector implements higher modes [140] and eccentricity [60] and can model hyperbolic mergers [141].

It is a time-domain waveform that has been used in GWTC-1 [3] for GW170817 and GWTC-2 [18]. TEOBResumS is available at [https://bitbucket.org/eob\\_ihes/teobresums/wiki/Home](https://bitbucket.org/eob_ihes/teobresums/wiki/Home) and included in its non-spinning, reduced-order modeling (ROM) version in the LAL's module [https://lscsoft.docs.ligo.org/lalsuite/lalsimulation/\\_l\\_a\\_l\\_sim\\_inspiral\\_t\\_e\\_o\\_b\\_resum\\_r\\_o\\_m\\_8c.html](https://lscsoft.docs.ligo.org/lalsuite/lalsimulation/_l_a_l_sim_inspiral_t_e_o_b_resum_r_o_m_8c.html).

## Phenomenological (IMRPhenom) models

In the frequency domain, phenomenological IMR (IMRPhenom) models have been presented as another way to construct full GW signals by combining the analytical PN/BHP results with NR simulations.

The IMRPhenom model basically consists of three parts: the PN inspiral (Ins) part, merger-ringdown (MR) part, and intermediate (Int) part between the former two parts. The amplitude  $A_{\text{IMR}}(f)$  and the GW phase  $\Phi_{\text{IMR}}(f)$  are written in the form of

$$\begin{aligned}\Phi_{\text{IMR}}(f) &= \phi_{\text{Ins}}(f) \theta_{f_{1\phi}}^- + \theta_{f_{1\phi}}^+ \phi_{\text{Int}}(f) \theta_{f_{2\phi}}^- + \theta_{f_{2\phi}}^+ \phi_{\text{MR}}(f), \\ A_{\text{IMR}}(f) &= A_{\text{Ins}}(f) \theta_{f_{1A}}^- + \theta_{f_{1A}}^+ A_{\text{Int}}(f) \theta_{f_{2A}}^- + \theta_{f_{2A}}^+ A_{\text{MR}}(f),\end{aligned}\quad (102)$$

where the function  $\theta_{f_0}^\pm$  is defined by

$$\theta_{f_0}^\pm = \frac{1}{2} \{1 \pm \theta(f - f_0)\}; \quad \theta(f - f_0) = \begin{cases} -1, & f < f_0, \\ 1, & f \geq f_0. \end{cases}\quad (103)$$

Here, we basically pattern after the notation in Refs. [105, 159], and we introduced the certainly prepared transition frequencies  $f_{1\phi}$ ,  $f_{2\phi}$ ,  $f_{1A}$  and  $f_{2A}$ .

Each individual component is parametrised and calibrated against NR simulations. For example, the amplitude and phase models of the inspiral part are based on extensions of those of TaylorF2 models with calibration parameters. Their model functions in the state-of-the-art PhenomX framework take the form [159]



$$\begin{aligned}
A_{\text{Ins}} &= A_{\text{TF2}} + \sqrt{\frac{2\eta}{3\pi^{1/3}}} f^{-7/6} \sum_{i=1}^3 \rho_i (\pi f)^{(6+i)/3}, \\
\phi_{\text{Ins}} &= \phi_{\text{TF2}} + \frac{1}{\eta} \left( \sigma_0 + \sigma_1 f + \frac{3}{4} \sigma_2 f^{4/3} + \frac{3}{5} \sigma_3 f^{5/3} + \frac{1}{2} \sigma_4 f^2 + \frac{3}{7} \sigma_5 f^{7/3} \right), \quad (104)
\end{aligned}$$

where  $A_{\text{TF2}}$  and  $\phi_{\text{TF2}}$  are (essentially) the same as TaylorF2 models in Eqs. (87) and (85). The free parameters  $\rho_i$  and  $\sigma_j$  ( $j = 0, 1, 2, 3, 4$  and  $5$ ) are phenomenological, pseudo-PN coefficients calibrated against NR data sets.

In Ref. [22], the first frequency-domain IMR waveform, IMRPhenomA model, was presented for non-spinning BBHs. The spinning, nonprecessing BBH waveform is called the IMRPhenomB model [23], and it is later improved to IMRPhenomC model [166]; see also Section II-b in Ref. [2] about IMRPhenomA/B models. In the classical GW data analysis of the LIGO fifth science run (S5) [2], the IMRPhenomA and IMRPhenomB models were used as an IMR theoretical template; note, however, that IMRPhenomA/B/C models have been deprecated and they are no longer used in the modern LAL simulation. All models in IMRPhenom family are available at [https://lscsoft.docs.ligo.org/lalsuite/lalsimulation/group\\_\\_l\\_a\\_l\\_sim\\_i\\_m\\_r\\_phenom\\_\\_c.html](https://lscsoft.docs.ligo.org/lalsuite/lalsimulation/group__l_a_l_sim_i_m_r_phenom__c.html)

### IMRPhenomD family

*IMRPhenomD/HM.*— In Refs. [105, 111], the IMRPhenomD model is presented for the dominant  $(\ell, |m|) = (2, 2)$  modes of spinning, nonprecessing binaries. For the analysis of GW170817 in Ref. [4], using the IMRPhenomD model with the help of NRTidal for the tidal effects approximants [79, 76, 77]

$$\text{IMRPhenomD\_NRTidal} = \text{IMRPhenomD} + \text{NRTidal}$$

was used as a signal model of BNSs. In Ref. [127], based on the IMRPhenomD model, the subdominant harmonic modes have been included in the waveform model, giving origin to the IMRPhenomHM model.

*IMRPhenomP/Pv2/Pv3/Pv3HM.*— The IMRPhenomP [96] and IMRPhenomPv2 models [105] are for precessing binaries, based on the nonprecessing IMRPhenomC and IMRPhenomD models, respectively, and have the single precession spin (to rotate the nonprecessing signals in the co-precession frame). The improved IMRPhenomPv3 model [112] has two independent spins in the precession dynamics, making use of the results of the multi-timescale analysis of the (conservative) PN precession dynamics [58] to cover a broader region of the parameter space than that of the IMRPhenomPv2 model; recall the radiation-reaction and precession time scales in Eqs. (32) and (90) that imply  $t_p/t_{\text{RR}} \sim v^3 \ll 1$ . This model is further extended to IMRPhenomPv3HM model [113] to include subdominant GW modes, which is based on the (nonprecessing) IMRPhenomHM model.

The IMRPhenomPv2 model was used in the detailed study on the properties of GW150914 [9]. In GWTC-1 [3], the IMRPhenomPv2 model was also used

as a model for BBH coalescence. The IMRPhenomPv3HM model was used for GW190521 [14] and GW190814 [15] as well as Ref. [13] and GWTC-2 [18] to analyse potential BBH signals (we note that a fast and accurate NR surrogate model NRSur7dq4 [180] has also been used for GW190521 and GWTC-2).

*IMRPhenomPv2\_NRTidal/NRTidalv2*.— Including spin-precessing with the Pv2 style [105] and tidal interactions with the NRTidal [76], we have

$$\text{IMRPhenomPv2\_NRTidal} = \text{IMRPhenomPv2} + \text{NRTidal}.$$

This is called as the IMRPhenomPv2\_NRTidal (PhenomPv2NRT) model [79]. In Ref. [77], an improved version of IMRPhenomPv2\_NRTidal has been presented as the IMRPhenomPv2\_NRTidalv2 model. In the detailed analysis of GW170817 [4], this IMRPhenomPv2\_NRTidal model has been used as the reference model. In GWTC-1 [3], this was used as a frequency-domain model for GW170817. Also, to analyze GW190425 [7] with total mass  $\sim 3.4M_{\odot}$  and any sources in GWTC-2 [18] that had evidence for at least one binary component below  $3M_{\odot}$ , this was used as the signal model.

*IMRPhenomNSBH*.— For spinning, nonprecessing NSBH binaries (with a non-spinning NS and a spinning BH), the IMRPhenomNSBH model has been developed [177], based on the amplitude of the IMRPhenomC model and the phase of the IMRPhenomD\_NRTidalv2 model. The IMRPhenomNSBH model was used for the analysis of GW190814 [15] and potential NSBH sources in GWTC-2 [18].

## IMRPhenomX family

IMRPhenomX family is an entirely new Phenom pipeline, superseding the IMRPhenomD family. The main improvements from PhenomD include, e.g., (i) the larger number of input NR waveforms for calibrations increased from 19 to 652, broadening the coverage of the mass ratio from 1 : 18 to 1 : 1000 with the help of BBH merger simulations in the small mass-ratio limit produced by EOB-BHP approach [97, 98, 99]; (ii) the higher dimensionality the model parameter space enlarged from 2 to 3, using the symmetric mass ratio and two spin components (orthogonal to the orbital plane); further improvements are summarized in Sec.X of Ref. [159]. These refinements resolve various shortcoming of PhenomD family and drastically improve the accuracy.

The baseline models for the dominant  $(\ell, m) = (2, 2)$  modes of spinning, nonprecessing binaries is called IMRPhenomXAS [159]. This model is then generalized to IMRPhenomXHM model [89, 90] to include subdominant harmonic modes of nonprecessing binaries, and further to the IMRPhenomXPHM model [160] for precessing binaries with “twisting-up” the nonprecessing waveform using the (Pv3-style) double-spin approach developed in Ref. [58].

All the models in IMRPhenomX family are available at [https://lscsoft.docs.ligo.org/lalsuite/lalsimulation/group\\_\\_\\_l\\_a\\_l\\_sim\\_i\\_m\\_r\\_phenom\\_x\\_\\_c.html](https://lscsoft.docs.ligo.org/lalsuite/lalsimulation/group___l_a_l_sim_i_m_r_phenom_x__c.html); see Appendix C of Ref. [89] for the technical de-

tails of implementations, leading to significantly faster waveform production without compromising on accuracy.

### **IMRPhenomTP**

IMRPhenomTP Ref. [80] is a time-domain phenomenological model for the dominant  $(\ell, m) = (2, 2)$  modes of spinning precessing BBHs, making use of the "twisting up" approximation [168] (see also, e.g., Section 5.3 of Ref. [95]) to the non-precessing BBHs, based on TaylorT3 approximants.

### **GIMR for modified theory of gravity**

Until now we have (implicitly) assumed that the gravity theory is described by Einstein's GR. However, it is not the only relativistic theory of gravity. Indeed, motivated by the recent observation of accelerating expansion of the universe, there is a growing interest to consider alternative gravity theory other than GR. Yet, each candidate gravity theory has to be experimentally verified, and the GW signals from the coalescence of a compact object binary allow a unique test of gravity theories in the strong curvature regime; this topic is covered in Chapter 41 by Yagi and Carson in this book with a lot more details.

Although we can consider model-dependent GW waveforms for each modified theory of gravity, it is possible to formulate a model-independent waveform that phenomenologically captures the main features of a wider class of the modified theory of gravity. For instance, the GIMR model is prepared by introducing deformations to the phase of the frequency-domain IMRPhenom waveform model in GR (see also a parametrized post-Einsteinian framework in Ref. [183]). The standard pipeline for model-independent GIMR waveforms is called TIGER (Test Infrastructure for General Relativity) [20]; see Chapter 44 by Broeck in this book for a detailed description.

In Refs. [10] for GW150914, [5] for GW170817, [6] for GWTC-1, and [17] for GWTC-2, the GIMR model has been also used to test the dipole radiation at  $-1$ PN order, which is absent in GR (recall our previous discussion on the quadrupole formalism for GW generation) but is a common prediction of modified theory of gravity due to the existence of additional scalar degrees of freedom mediating long-range interactions. See Chapter 40 by De Laurentis and De Martino in this book for more details.

## **Conclusion**

The development of the theoretical GW templates of coalescing compact object binaries was initiated within the PN approach, focusing on the adiabatic inspiral phase.

However, after the 2005 breakthroughs in NR simulations of BBHs [161, 55, 31] and the observations of GW events by LIGO and Virgo, learning that almost all the GW signals detected so far have both merger and ringdown in the sensitive frequency band of LIGO, Virgo and KAGRA, complete models with inspiral, merger, and ring-down phases are under vigorous development.

The theoretical construction of GW waveforms for the entire coalescence makes full use of known analytical approximation scheme to other methods than the PN approximation to GR, e.g. the BHP (and self-force) theory as well as cutting-edge NR simulations.

This motivation has continuously driven a concerted effort by GW theorists and data analysts to develop accurate and efficient waveforms of compact-object binary mergers [126], and we have provided a broad (but yet small-corner) overview of this active subject. We conclude our chapter by listing some of open challenges and prospects.

- Although we have exclusively discussed quasicircular binaries in this chapter, the observation of nonzero eccentricity will be a smoking gun of the formation scenario of binary systems: evolution of isolated binaries (e.g., circularized by binary interactions and GW radiation; recall Eq. (89)) versus dynamically formed binaries in dense stellar environments (e.g., the Kozai-Lidov mechanism [116, 125]).
- The ground-based GW detectors, LIGO, Virgo, and KAGRA, have a peak of sensitivity around 100 Hz. For future plans of ground-based detectors, e.g., KAGRA+ [133], Voyager (<https://dcc.ligo.org/LIGO-G1602258/public>), Einstein Telescope [101] and Cosmic Explorer [163], significant sensitivity improvements are expected both in low- and high-frequency bands. Enhanced low-frequency part would stretch the visible range of BBHs and NS-BH inspirals to heavier masses. At the same time, improvements in the high frequency part would enable us to observe the BNS merger phase more accurately, where the (equation-of-state dependent) finite-size effects of NSs become particularly pronounced.
- The observation of GW190814 showed a binary system with mass ratio around 10:1. The remnant compact object of GW190521 [14] has been considered as an intermediate mass BH. The combination of these two events may suggest the existence of intermediate mass black holes and the possibility to observe in the future binary systems with an individual mass ratio around 1 : 100. In LAL-Simulation [126], a program for “extreme” mass ratios is present at [https://lscsoft.docs.ligo.org/lalsuite/lalsimulation/group\\_\\_l\\_a\\_l\\_sim\\_i\\_m\\_r\\_phenom\\_x\\_\\_c.html](https://lscsoft.docs.ligo.org/lalsuite/lalsimulation/group__l_a_l_sim_i_m_r_phenom_x__c.html), calibrated to NR waveforms for mass ratio from  $q = 1$  to 20, and the region between  $q = 20$  and 1000, where no NR waveforms are available, is covered by the waveform of extreme mass-ratio inspirals (EMRIs) (based on the BHP theory with the EOB orbital dynamics in the small mass-ratio limit [97, 98, 99]), with the mass ratio region  $200 < q < 1000$  covered by the extrapolation based on these waveforms. Further synergy with EMRI waveforms is ongoing: see, e.g., Refs. [38, 164, 131] and references therein.

- The planned space-based GW observatory, e.g., LISA [29], (B-)DECIGO [110, 171, 144], and TianQin [132] will observe much longer-length inspiral signals of compact object binaries than LIGO, Virgo and KAGRA. They will allow us to measure the binary parameters with exquisite precision, particularly in the context of the multiband GW astronomy [170, 181, 107]. At the same time, however, the benefit of such an observation is gained only when one is able to construct much more accurate templates for the inspiral phase than currently available models: their phase coherence has to be maintained over  $O(10^6)$  GW cycles (and one should also devise a consistent data analysis technique to process such a long-length GW signals).
- Our presentation does not cover the *efficiency* aspects in the waveform modelling. The matched-filtering search of GW signal needs a (so named) “template bank” by nature (see, e.g., Chapter 43 by Krolak in this book), designed to efficiently cover a parameter space as large as possible. This is a computationally expensive and challenging task, demanding different investigations. A common strategy is to use “effective” parameters such as the chirp mass  $\mathcal{M}$  (27), the reduced spin  $\chi_{\text{PN}}$  (88), and the binary tidal deformability  $\tilde{\Lambda}$  (95), to reduce the numbers of the dimension in the parameter space by focusing on those combinations of astrophysical parameters which affect most prominently the waveform. An alternative strategy is a reduced-order modeling (ROM) [162] and a surrogate model (for NR waveforms) [180].

## Acknowledgments

The authors warmly thank Maria Haney for reading the manuscript and improving it with her suggestions. S. I. acknowledges support from STFC through Grant No. ST/R00045X/1. S. I. also thanks the financial support from the Ministry of Education, MEC, during his stay at IIP-Natal-Brazil and acknowledges networking support by the GWverse COST Action CA16104, “Black holes, gravitational waves and fundamental physics.” The work of R. S. is partially supported by CNPq. H. N. acknowledges support from JSPS KAKENHI Grant Nos. JP16K05347 and JP17H06358.

## References

- [1] Aasi J, et al (2015) Advanced LIGO. *Class Quant Grav* 32:074001, DOI 10.1088/0264-9381/32/7/074001, [1411.4547](https://doi.org/10.1088/0264-9381/32/7/074001)
- [2] Abadie J, et al (2011) Search for gravitational waves from binary black hole inspiral, merger and ringdown. *Phys Rev D* 83:122005, DOI 10.1103/PhysRevD.86.069903, 10.1103/PhysRevD.85.089904, 10.

- 1103/PhysRevD.83.122005, [Erratum: Phys. Rev.D86,069903(2012)], [1102.3781](#)
- [3] Abbott B, et al (2019) GWTC-1: A Gravitational-Wave Transient Catalog of Compact Binary Mergers Observed by LIGO and Virgo during the First and Second Observing Runs. Phys Rev X 9(3):031040, DOI 10.1103/PhysRevX.9.031040, [1811.12907](#)
- [4] Abbott B, et al (2019) Properties of the binary neutron star merger GW170817. Phys Rev X 9(1):011001, DOI 10.1103/PhysRevX.9.011001, [1805.11579](#)
- [5] Abbott B, et al (2019) Tests of General Relativity with GW170817. Phys Rev Lett 123(1):011102, DOI 10.1103/PhysRevLett.123.011102, [1811.00364](#)
- [6] Abbott B, et al (2019) Tests of General Relativity with the Binary Black Hole Signals from the LIGO-Virgo Catalog GWTC-1. Phys Rev D 100(10):104036, DOI 10.1103/PhysRevD.100.104036, [1903.04467](#)
- [7] Abbott B, et al (2020) GW190425: Observation of a Compact Binary Coalescence with Total Mass  $\sim 3.4M_{\odot}$ . Astrophys J Lett 892:L3, DOI 10.3847/2041-8213/ab75f5, [2001.01761](#)
- [8] Abbott BP, et al (2016) Observation of Gravitational Waves from a Binary Black Hole Merger. Phys Rev Lett 116(6):061102, DOI 10.1103/PhysRevLett.116.061102, [1602.03837](#)
- [9] Abbott BP, et al (2016) Properties of the Binary Black Hole Merger GW150914. Phys Rev Lett 116(24):241102, DOI 10.1103/PhysRevLett.116.241102, [1602.03840](#)
- [10] Abbott BP, et al (2016) Tests of general relativity with GW150914. Phys Rev Lett 116(22):221101, DOI 10.1103/PhysRevLett.116.221101, 10.1103/PhysRevLett.121.129902, [Erratum: Phys. Rev. Lett.121,no.12,129902(2018)], [1602.03841](#)
- [11] Abbott BP, et al (2017) GW170817: Observation of Gravitational Waves from a Binary Neutron Star Inspiral. Phys Rev Lett 119(16):161101, DOI 10.1103/PhysRevLett.119.161101, [1710.05832](#)
- [12] Abbott BP, et al (2017) The basic physics of the binary black hole merger GW150914. Annalen Phys 529(1-2):1600209, DOI 10.1002/andp.201600209, [1608.01940](#)
- [13] Abbott R, et al (2020) GW190412: Observation of a Binary-Black-Hole Coalescence with Asymmetric Masses. Phys Rev D 102(4):043015, DOI 10.1103/PhysRevD.102.043015, [2004.08342](#)
- [14] Abbott R, et al (2020) GW190521: A Binary Black Hole Merger with a Total Mass of  $150 M_{\odot}$ . Phys Rev Lett 125:101102, DOI 10.1103/PhysRevLett.125.101102, [2009.01075](#)
- [15] Abbott R, et al (2020) GW190814: Gravitational Waves from the Coalescence of a 23 Solar Mass Black Hole with a 2.6 Solar Mass Compact Object. Astrophys J 896(2):L44, DOI 10.3847/2041-8213/ab960f, [2006.12611](#)
- [16] Abbott R, et al (2020) Properties and Astrophysical Implications of the  $150 M_{\odot}$  Binary Black Hole Merger GW190521. Astrophys J 900(1):L13, DOI 10.3847/2041-8213/aba493, [2009.01190](#)

- [17] Abbott R, et al (2020) Tests of General Relativity with Binary Black Holes from the second LIGO-Virgo Gravitational-Wave Transient Catalog. arXiv e-prints arXiv:2010.14529, [2010.14529](#)
- [18] Abbott R, et al (2021) GWTC-2: Compact Binary Coalescences Observed by LIGO and Virgo During the First Half of the Third Observing Run. Phys Rev X 11:021053, DOI 10.1103/PhysRevX.11.021053, [2010.14527](#)
- [19] Acernese F, et al (2015) Advanced Virgo: a second-generation interferometric gravitational wave detector. Class Quant Grav 32(2):024001, DOI 10.1088/0264-9381/32/2/024001, [1408.3978](#)
- [20] Agathos M, Del Pozzo W, Li TGF, Van Den Broeck C, Veitch J, Vitale S (2014) TIGER: A data analysis pipeline for testing the strong-field dynamics of general relativity with gravitational wave signals from coalescing compact binaries. Phys Rev D 89(8):082001, DOI 10.1103/PhysRevD.89.082001, [1311.0420](#)
- [21] Ajith P (2011) Addressing the spin question in gravitational-wave searches: Waveform templates for inspiralling compact binaries with nonprecessing spins. Phys Rev D 84:084037, DOI 10.1103/PhysRevD.84.084037, [1107.1267](#)
- [22] Ajith P, et al (2008) A Template bank for gravitational waveforms from coalescing binary black holes. I. Non-spinning binaries. Phys Rev D 77:104017, DOI 10.1103/PhysRevD.77.104017, [Erratum: Phys.Rev.D 79, 129901 (2009)], [0710.2335](#)
- [23] Ajith P, et al (2011) Inspiral-merger-ringdown waveforms for black-hole binaries with non-precessing spins. Phys Rev Lett 106:241101, DOI 10.1103/PhysRevLett.106.241101, [0909.2867](#)
- [24] Ajith P, et al (2012) The NINJA-2 catalog of hybrid post-Newtonian/numerical-relativity waveforms for non-precessing black-hole binaries. Class Quant Grav 29:124001, DOI 10.1088/0264-9381/30/19/199401,10.1088/0264-9381/29/12/124001, [Erratum: Class. Quant. Grav.30,199401(2013)], [1201.5319](#)
- [25] Akcay S, Bernuzzi S, Messina F, Nagar A, Ortiz N, Rettengo P (2019) Effective-one-body multipolar waveform for tidally interacting binary neutron stars up to merger. Phys Rev D 99(4):044051, DOI 10.1103/PhysRevD.99.044051, [1812.02744](#)
- [26] Akcay S, Gamba R, Bernuzzi S (2021) Hybrid post-Newtonian effective-one-body scheme for spin-precessing compact-binary waveforms up to merger. Phys Rev D 103(2):024014, DOI 10.1103/PhysRevD.103.024014, [2005.05338](#)
- [27] Akutsu T, et al (2020) Overview of KAGRA: Detector design and construction history. arXiv e-prints arXiv:2005.05574, [2005.05574](#)
- [28] Allen B, Anderson WG, Brady PR, Brown DA, Creighton JD (2012) FIND-CHIRP: An Algorithm for detection of gravitational waves from inspiraling compact binaries. Phys Rev D 85:122006, DOI 10.1103/PhysRevD.85.122006, [gr-qc/0509116](#)

- [29] Amaro-Seoane P, et al (2017) Laser Interferometer Space Antenna. arXiv e-prints arXiv:1702.00786, [1702.00786](#)
- [30] Antonelli A, van de Meent M, Buonanno A, Steinhoff J, Vines J (2020) Quasicircular inspirals and plunges from nonspinning effective-one-body Hamiltonians with gravitational self-force information. *Phys Rev D* 101(2):024024, DOI 10.1103/PhysRevD.101.024024, [1907.11597](#)
- [31] Baker JG, Centrella J, Choi DI, Koppitz M, van Meter J (2006) Gravitational wave extraction from an inspiraling configuration of merging black holes. *Phys Rev Lett* 96:111102, DOI 10.1103/PhysRevLett.96.111102, [gr-qc/0511103](#)
- [32] Barack L, Pound A (2019) Self-force and radiation reaction in general relativity. *Rept Prog Phys* 82(1):016904, DOI 10.1088/1361-6633/aae552, [1805.10385](#)
- [33] Bardeen JM, Press WH, Teukolsky SA (1972) Rotating black holes: Locally nonrotating frames, energy extraction, and scalar synchrotron radiation. *Astrophys J* 178:347, DOI 10.1086/151796
- [34] Baumgarte TW, Shapiro SL (2010) *Numerical Relativity: Solving Einstein's Equations on the Computer*. Cambridge University Press, DOI 10.1017/CBO9781139193344
- [35] Bernard L, Blanchet L, Faye G, Marchand T (2018) Center-of-Mass Equations of Motion and Conserved Integrals of Compact Binary Systems at the Fourth Post-Newtonian Order. *Phys Rev D* 97(4):044037, DOI 10.1103/PhysRevD.97.044037, [1711.00283](#)
- [36] Bernuzzi S, Nagar A, Thierfelder M, Brugmann B (2012) Tidal effects in binary neutron star coalescence. *Phys Rev D* 86:044030, DOI 10.1103/PhysRevD.86.044030, [1205.3403](#)
- [37] Bernuzzi S, Nagar A, Dietrich T, Damour T (2015) Modeling the Dynamics of Tidally Interacting Binary Neutron Stars up to the Merger. *Phys Rev Lett* 114(16):161103, DOI 10.1103/PhysRevLett.114.161103, [1412.4553](#)
- [38] Berry C, Hughes S, Sopuerta C, Chua A, Heffernan A, Holley-Bockelmann K, Mihaylov D, Miller C, Sesana A (2019) The unique potential of extreme mass-ratio inspirals for gravitational-wave astronomy. *Bulletin of the AAS* 51(3):42, [1903.03686](#)
- [39] Berti E, Cardoso V, Starinets AO (2009) Quasinormal modes of black holes and black branes. *Class Quant Grav* 26:163001, DOI 10.1088/0264-9381/26/16/163001, [0905.2975](#)
- [40] Berti E, Yagi K, Yang H, Yunes N (2018) Extreme Gravity Tests with Gravitational Waves from Compact Binary Coalescences: (II) Ringdown. *Gen Rel Grav* 50(5):49, DOI 10.1007/s10714-018-2372-6, [1801.03587](#)
- [41] Binnington T, Poisson E (2009) Relativistic theory of tidal Love numbers. *Phys Rev D* 80:084018, DOI 10.1103/PhysRevD.80.084018, [0906.1366](#)
- [42] Blanchet L (2014) Gravitational Radiation from Post-Newtonian Sources and Inspiralling Compact Binaries. *Living Rev Rel* 17:2, DOI 10.12942/lrr-2014-2, [1310.1528](#)



- [43] Blanchet L, Buonanno A, Le Tiec A (2013) First law of mechanics for black hole binaries with spins. *Phys Rev D* 87(2):024030, DOI 10.1103/PhysRevD.87.024030, [1211.1060](#)
- [44] Bohe A, Marsat S, Faye G, Blanchet L (2013) Next-to-next-to-leading order spin-orbit effects in the near-zone metric and precession equations of compact binaries. *Class Quant Grav* 30:075017, DOI 10.1088/0264-9381/30/7/075017, [1212.5520](#)
- [45] Bohé A, et al (2017) Improved effective-one-body model of spinning, non-precessing binary black holes for the era of gravitational-wave astrophysics with advanced detectors. *Phys Rev D* 95(4):044028, DOI 10.1103/PhysRevD.95.044028, [1611.03703](#)
- [46] Boyle M, Brown DA, Kidder LE, Mroue AH, Pfeiffer HP, Scheel MA, Cook GB, Teukolsky SA (2007) High-accuracy comparison of numerical relativity simulations with post-Newtonian expansions. *Phys Rev D* 76:124038, DOI 10.1103/PhysRevD.76.124038, [0710.0158](#)
- [47] Boyle M, et al (2019) The SXS Collaboration catalog of binary black hole simulations. *Class Quant Grav* 36(19):195006, DOI 10.1088/1361-6382/ab34e2, [1904.04831](#)
- [48] Breschi M, Bernuzzi S, Zappa F, Agathos M, Perego A, Radice D, Nagar A (2019) kiloHertz gravitational waves from binary neutron star remnants: time-domain model and constraints on extreme matter. *Phys Rev D* 100(10):104029, DOI 10.1103/PhysRevD.100.104029, [1908.11418](#)
- [49] Buonanno A, Damour T (1999) Effective one-body approach to general relativistic two-body dynamics. *Phys Rev D* 59:084006, DOI 10.1103/PhysRevD.59.084006, [gr-qc/9811091](#)
- [50] Buonanno A, Damour T (2000) Transition from inspiral to plunge in binary black hole coalescences. *Phys Rev D* 62:064015, DOI 10.1103/PhysRevD.62.064015, [gr-qc/0001013](#)
- [51] Buonanno A, Chen Yb, Vallisneri M (2003) Detecting gravitational waves from precessing binaries of spinning compact objects: Adiabatic limit. *Phys Rev D* 67:104025, DOI 10.1103/PhysRevD.67.104025, 10.1103/PhysRevD.74.029904, [Erratum: *Phys. Rev.D*74,029904(2006)], [gr-qc/0211087](#)
- [52] Buonanno A, Chen Y, Damour T (2006) Transition from inspiral to plunge in precessing binaries of spinning black holes. *Phys Rev D* 74:104005, DOI 10.1103/PhysRevD.74.104005, [gr-qc/0508067](#)
- [53] Buonanno A, Pan Y, Baker JG, Centrella J, Kelly BJ, McWilliams ST, van Meter JR (2007) Toward faithful templates for non-spinning binary black holes using the effective-one-body approach. *Phys Rev D* 76:104049, DOI 10.1103/PhysRevD.76.104049, [0706.3732](#)
- [54] Buonanno A, Iyer B, Ochsner E, Pan Y, Sathyaprakash B (2009) Comparison of post-Newtonian templates for compact binary inspiral signals in gravitational-wave detectors. *Phys Rev D* 80:084043, DOI 10.1103/PhysRevD.80.084043, [0907.0700](#)

- [55] Campanelli M, Lousto C, Marronetti P, Zlochower Y (2006) Accurate evolutions of orbiting black-hole binaries without excision. *Phys Rev Lett* 96:111101, DOI 10.1103/PhysRevLett.96.111101, [gr-qc/0511048](#)
- [56] Chatziioannou K (2020) Neutron star tidal deformability and equation of state constraints. *Gen Rel Grav* 52(11):109, DOI 10.1007/s10714-020-02754-3, [2006.03168](#)
- [57] Chatziioannou K, Poisson E, Yunes N (2016) Improved next-to-leading order tidal heating and torquing of a Kerr black hole. *Phys Rev D* 94(8):084043, DOI 10.1103/PhysRevD.94.084043, [1608.02899](#)
- [58] Chatziioannou K, Klein A, Yunes N, Cornish N (2017) Constructing Gravitational Waves from Generic Spin-Precessing Compact Binary Inspirals. *Phys Rev D* 95(10):104004, DOI 10.1103/PhysRevD.95.104004, [1703.03967](#)
- [59] Chia HS (2020) Tidal Deformation and Dissipation of Rotating Black Holes. arXiv e-prints arXiv:2010.07300, [2010.07300](#)
- [60] Chiamello D, Nagar A (2020) Faithful analytical effective-one-body waveform model for spin-aligned, moderately eccentric, coalescing black hole binaries. *Phys Rev D* 101(10):101501, DOI 10.1103/PhysRevD.101.101501, [2001.11736](#)
- [61] Collaboration LS (2020) LALSuite documentation, v. 2.2.0.1. URL [https://lscsoft.docs.ligo.org/lalsuite/lalsimulation/group\\_\\_l\\_a\\_l\\_sim\\_inspiral\\_\\_h.html](https://lscsoft.docs.ligo.org/lalsuite/lalsimulation/group__l_a_l_sim_inspiral__h.html)
- [62] Cotesta R, Buonanno A, Bohe A, Taracchini A, Hinder I, Ossokine S (2018) Enriching the Symphony of Gravitational Waves from Binary Black Holes by Tuning Higher Harmonics. *Phys Rev D* 98(8):084028, DOI 10.1103/PhysRevD.98.084028, [1803.10701](#)
- [63] Cutler C, et al (1993) The Last three minutes: issues in gravitational wave measurements of coalescing compact binaries. *Phys Rev Lett* 70:2984–2987, DOI 10.1103/PhysRevLett.70.2984, [astro-ph/9208005](#)
- [64] Damour T (1984) *The Motion of Compact Bodies and Gravitational Radiation*, Springer Netherlands, Dordrecht, pp 89–106. DOI 10.1007/978-94-009-6469-3\_7, URL [https://doi.org/10.1007/978-94-009-6469-3\\_7](https://doi.org/10.1007/978-94-009-6469-3_7)
- [65] Damour T (2001) Coalescence of two spinning black holes: an effective one-body approach. *Phys Rev D* 64:124013, DOI 10.1103/PhysRevD.64.124013, [gr-qc/0103018](#)
- [66] Damour T (2008) Introductory lectures on the Effective One Body formalism. *Int J Mod Phys A* 23:1130–1148, DOI 10.1142/S0217751X08039992, [0802.4047](#)
- [67] Damour T (2014) The General Relativistic Two Body Problem and the Effective One Body Formalism. *Fundam Theor Phys* 177:111–145, DOI 10.1007/978-3-319-06349-2\_5, [1212.3169](#)
- [68] Damour T (2016) Gravitational scattering, post-Minkowskian approximation and Effective One-Body theory. *Phys Rev D* 94(10):104015, DOI 10.1103/PhysRevD.94.104015, [1609.00354](#)

- [69] Damour T, Lecian OM (2009) On the gravitational polarizability of black holes. *Phys Rev D* 80:044017, DOI 10.1103/PhysRevD.80.044017, [0906.3003](#)
- [70] Damour T, Nagar A (2007) Faithful effective-one-body waveforms of small-mass-ratio coalescing black-hole binaries. *Phys Rev D* 76:064028, DOI 10.1103/PhysRevD.76.064028, [0705.2519](#)
- [71] Damour T, Nagar A (2008) Comparing Effective-One-Body gravitational waveforms to accurate numerical data. *Phys Rev D* 77:024043, DOI 10.1103/PhysRevD.77.024043, [0711.2628](#)
- [72] Damour T, Iyer BR, Sathyaprakash BS (2001) A Comparison of search templates for gravitational waves from binary inspiral. *Phys Rev D* 63:044023, DOI 10.1103/PhysRevD.63.044023, 10.1103/PhysRevD.72.029902, [Erratum: *Phys. Rev.D*72,029902(2005)], [gr-qc/0010009](#)
- [73] Damour T, Iyer BR, Sathyaprakash BS (2002) A Comparison of search templates for gravitational waves from binary inspiral - 3.5PN update. *Phys Rev D* 66:027502, DOI 10.1103/PhysRevD.66.027502, [gr-qc/0207021](#)
- [74] Damour T, Iyer BR, Nagar A (2009) Improved resummation of post-Newtonian multipolar waveforms from circularized compact binaries. *Phys Rev D* 79:064004, DOI 10.1103/PhysRevD.79.064004, [0811.2069](#)
- [75] Damour T, Jaranowski P, Schäfer G (2015) Fourth post-Newtonian effective one-body dynamics. *Phys Rev D* 91(8):084024, DOI 10.1103/PhysRevD.91.084024, [1502.07245](#)
- [76] Dietrich T, Bernuzzi S, Tichy W (2017) Closed-form tidal approximants for binary neutron star gravitational waveforms constructed from high-resolution numerical relativity simulations. *Phys Rev D* 96(12):121501, DOI 10.1103/PhysRevD.96.121501, [1706.02969](#)
- [77] Dietrich T, Samajdar A, Khan S, Johnson-McDaniel NK, Dudi R, Tichy W (2019) Improving the NRTidal model for binary neutron star systems. *Phys Rev D* 100(4):044003, DOI 10.1103/PhysRevD.100.044003, [1905.06011](#)
- [78] Dietrich T, Hinderer T, Samajdar A (2021) Interpreting Binary Neutron Star Mergers: Describing the Binary Neutron Star Dynamics, Modelling Gravitational Waveforms, and Analyzing Detections. *Gen Rel Grav* 53(3):27, DOI 10.1007/s10714-020-02751-6, [2004.02527](#)
- [79] Dietrich T, et al (2019) Matter imprints in waveform models for neutron star binaries: Tidal and self-spin effects. *Phys Rev D* 99(2):024029, DOI 10.1103/PhysRevD.99.024029, [1804.02235](#)
- [80] Estellés H, Ramos-Buades A, Husa S, García-Quirós C, Colleoni M, Haegel L, Jaume R (2020) IMRPhenomTP: A phenomenological time domain model for dominant quadrupole gravitational wave signal of coalescing binary black holes. arXiv e-prints arXiv:2004.08302, [2004.08302](#)
- [81] Field SE, Galley CR, Hesthaven JS, Kaye J, Tiglio M (2014) Fast prediction and evaluation of gravitational waveforms using surrogate models. *Phys Rev X* 4(3):031006, DOI 10.1103/PhysRevX.4.031006, [1308.3565](#)

- [82] Flanagan EE, Hinderer T (2008) Constraining neutron star tidal Love numbers with gravitational wave detectors. *Phys Rev D* 77:021502, DOI 10.1103/PhysRevD.77.021502, [0709.1915](#)
- [83] Flanagan EE, Hughes SA (2005) The Basics of gravitational wave theory. *New J Phys* 7:204, DOI 10.1088/1367-2630/7/1/204, [gr-qc/0501041](#)
- [84] Foffa S, Sturani R (2014) Effective field theory methods to model compact binaries. *Class Quant Grav* 31(4):043001, DOI 10.1088/0264-9381/31/4/043001, [1309.3474](#)
- [85] Foffa S, Sturani R (2019) Conservative dynamics of binary systems to fourth Post-Newtonian order in the EFT approach I: Regularized Lagrangian. *Phys Rev D* 100(2):024047, DOI 10.1103/PhysRevD.100.024047, [1903.05113](#)
- [86] Fujita R (2015) Gravitational Waves from a Particle in Circular Orbits around a Rotating Black Hole to the 11th Post-Newtonian Order. *PTEP* 2015(3):033E01, DOI 10.1093/ptep/ptv012, [1412.5689](#)
- [87] Fujita R, Isoyama S, Le Tiec A, Nakano H, Sago N, Tanaka T (2017) Hamiltonian Formulation of the Conservative Self-Force Dynamics in the Kerr Geometry. *Class Quant Grav* 34(13):134001, DOI 10.1088/1361-6382/aa7342, [1612.02504](#)
- [88] Futamase T, Itoh Y (2007) The post-Newtonian approximation for relativistic compact binaries. *Living Rev Rel* 10:2, DOI 10.12942/lrr-2007-2
- [89] García-Quirós C, Colleoni M, Husa S, Estellés H, Pratten G, Ramos-Buades A, Mateu-Lucena M, Jaume R (2020) IMRPhenomXHM: A multi-mode frequency-domain model for the gravitational wave signal from non-precessing black-hole binaries. *Phys Rev D* 102(6):064002, DOI 10.1103/PhysRevD.102.064002, [2001.10914](#)
- [90] García-Quirós C, Husa S, Mateu-Lucena M, Borchers A (2021) Accelerating the evaluation of inspiral–merger–ringdown waveforms with adapted grids. *Class Quant Grav* 38(1):015006, DOI 10.1088/1361-6382/abc36e, [2001.10897](#)
- [91] Goldberger WD (2007) Les Houches lectures on effective field theories and gravitational radiation. In: *Les Houches Summer School - Session 86: Particle Physics and Cosmology: The Fabric of Spacetime*, [hep-ph/0701129](#)
- [92] Goldberger WD, Rothstein IZ (2006) An Effective field theory of gravity for extended objects. *Phys Rev D* 73:104029, DOI 10.1103/PhysRevD.73.104029, [hep-th/0409156](#)
- [93] Goldberger WD, Rothstein IZ (2020) Horizon radiation reaction forces. *JHEP* 10:026, DOI 10.1007/JHEP10(2020)026, [2007.00731](#)
- [94] Gürlebeck N (2015) No-hair theorem for Black Holes in Astrophysical Environments. *Phys Rev Lett* 114(15):151102, DOI 10.1103/PhysRevLett.114.151102, [1503.03240](#)
- [95] Hannam M (2014) Modelling gravitational waves from precessing black-hole binaries: Progress, challenges and prospects. *Gen Rel Grav* 46:1767, DOI 10.1007/s10714-014-1767-2, [1312.3641](#)
- [96] Hannam M, Schmidt P, Bohé A, Haegel L, Husa S, Ohme F, Pratten G, Pürrer M (2014) Simple Model of Complete Precessing Black-Hole-Binary

- Gravitational Waveforms. *Phys Rev Lett* 113(15):151101, DOI 10.1103/PhysRevLett.113.151101, [1308.3271](#)
- [97] Harms E, Bernuzzi S, Nagar A, Zenginoglu A (2014) A new gravitational wave generation algorithm for particle perturbations of the Kerr spacetime. *Class Quant Grav* 31(24):245004, DOI 10.1088/0264-9381/31/24/245004, [1406.5983](#)
- [98] Harms E, Lukes-Gerakopoulos G, Bernuzzi S, Nagar A (2016) Asymptotic gravitational wave fluxes from a spinning particle in circular equatorial orbits around a rotating black hole. *Phys Rev D* 93(4):044015, DOI 10.1103/PhysRevD.93.044015, [Addendum: *Phys.Rev.D* 100, 129901 (2019)], [1510.05548](#)
- [99] Harms E, Lukes-Gerakopoulos G, Bernuzzi S, Nagar A (2016) Spinning test body orbiting around a Schwarzschild black hole: Circular dynamics and gravitational-wave fluxes. *Phys Rev D* 94(10):104010, DOI 10.1103/PhysRevD.94.104010, [1609.00356](#)
- [100] Harry I, Hinderer T (2018) Observing and measuring the neutron-star equation-of-state in spinning binary neutron star systems. *Class Quant Grav* 35(14):145010, DOI 10.1088/1361-6382/aac7e3, [1801.09972](#)
- [101] Hild S, Chelkowski S, Freise A (2008) Pushing towards the ET sensitivity using 'conventional' technology. arXiv e-prints arXiv:0810.0604, [0810.0604](#)
- [102] Hinderer T, et al (2016) Effects of neutron-star dynamic tides on gravitational waveforms within the effective-one-body approach. *Phys Rev Lett* 116(18):181101, DOI 10.1103/PhysRevLett.116.181101, [1602.00599](#)
- [103] Huerta EA, Kumar P, McWilliams ST, O'Shaughnessy R, Yunes N (2014) Accurate and efficient waveforms for compact binaries on eccentric orbits. *Phys Rev D* 90(8):084016, DOI 10.1103/PhysRevD.90.084016, [1408.3406](#)
- [104] Hughes SA (2019) Bound orbits of a slowly evolving black hole. *Phys Rev D* 100(6):064001, DOI 10.1103/PhysRevD.100.064001, [1806.09022](#)
- [105] Husa S, Khan S, Hannam M, Pürrer M, Ohme F, Jiménez Forteza X, Bohé A (2016) Frequency-domain gravitational waves from nonprecessing black-hole binaries. I. New numerical waveforms and anatomy of the signal. *Phys Rev D* 93(4):044006, DOI 10.1103/PhysRevD.93.044006, [1508.07250](#)
- [106] Isoyama S, Nakano H (2018) Post-Newtonian templates for binary black-hole inspirals: the effect of the horizon fluxes and the secular change in the black-hole masses and spins. *Class Quant Grav* 35(2):024001, DOI 10.1088/1361-6382/aa96c5, [1705.03869](#)
- [107] Isoyama S, Nakano H, Nakamura T (2018) Multiband Gravitational-Wave Astronomy: Observing binary inspirals with a decihertz detector, B-DECIGO. *PTEP* 2018(7):073E01, DOI 10.1093/ptep/pty078, [1802.06977](#)
- [108] Jaranowski P, Schäfer G (2015) Derivation of local-in-time fourth post-Newtonian ADM Hamiltonian for spinless compact binaries. *Phys Rev D* 92(12):124043, DOI 10.1103/PhysRevD.92.124043, [1508.01016](#)
- [109] Kawaguchi K, Kiuchi K, Kyutoku K, Sekiguchi Y, Shibata M, Taniguchi K (2018) Frequency-domain gravitational waveform models for inspiraling bi-

- nary neutron stars. *Phys Rev D* 97(4):044044, DOI 10.1103/PhysRevD.97.044044, [1802.06518](#)
- [110] Kawamura S, et al (2020) Current status of space gravitational wave antenna DECIGO and B-DECIGO. arXiv e-prints arXiv:2006.13545, [2006.13545](#)
- [111] Khan S, Husa S, Hannam M, Ohme F, Pürrer M, Jiménez Forteza X, Bohé A (2016) Frequency-domain gravitational waves from nonprecessing black-hole binaries. II. A phenomenological model for the advanced detector era. *Phys Rev D* 93(4):044007, DOI 10.1103/PhysRevD.93.044007, [1508.07253](#)
- [112] Khan S, Chatziioannou K, Hannam M, Ohme F (2019) Phenomenological model for the gravitational-wave signal from precessing binary black holes with two-spin effects. *Phys Rev D* 100(2):024059, DOI 10.1103/PhysRevD.100.024059, [1809.10113](#)
- [113] Khan S, Ohme F, Chatziioannou K, Hannam M (2020) Including higher order multipoles in gravitational-wave models for precessing binary black holes. *Phys Rev D* 101(2):024056, DOI 10.1103/PhysRevD.101.024056, [1911.06050](#)
- [114] Kokkotas KD, Schmidt BG (1999) Quasinormal modes of stars and black holes. *Living Rev Rel* 2:2, DOI 10.12942/lrr-1999-2, [gr-qc/9909058](#)
- [115] Kol B, Smolkin M (2012) Black hole stereotyping: Induced gravito-static polarization. *JHEP* 02:010, DOI 10.1007/JHEP02(2012)010, [1110.3764](#)
- [116] Kozai Y (1962) Secular perturbations of asteroids with high inclination and eccentricity. *Astron J* 67:591–598, DOI 10.1086/108790
- [117] Krishnendu N, Arun K, Mishra CK (2017) Testing the binary black hole nature of a compact binary coalescence. *Phys Rev Lett* 119(9):091101, DOI 10.1103/PhysRevLett.119.091101, [1701.06318](#)
- [118] Laarakkers WG, Poisson E (1999) Quadrupole moments of rotating neutron stars. *Astrophys J* 512:282–287, DOI 10.1086/306732, [gr-qc/9709033](#)
- [119] Landau L, Lifschits E (1975) *The Classical Theory of Fields*, Course of Theoretical Physics, vol Volume 2. Pergamon Press, Oxford
- [120] Le Tiec A (2014) The Overlap of Numerical Relativity, Perturbation Theory and Post-Newtonian Theory in the Binary Black Hole Problem. *Int J Mod Phys D* 23(10):1430022, DOI 10.1142/S0218271814300225, [1408.5505](#)
- [121] Le Tiec A, Casals M (2021) Spinning Black Holes Fall in Love. *Phys Rev Lett* 126(13):131102, DOI 10.1103/PhysRevLett.126.131102, [2007.00214](#)
- [122] Le Tiec A, Blanchet L, Whiting BF (2012) The First Law of Binary Black Hole Mechanics in General Relativity and Post-Newtonian Theory. *Phys Rev D* 85:064039, DOI 10.1103/PhysRevD.85.064039, [1111.5378](#)
- [123] Levi M (2020) Effective Field Theories of Post-Newtonian Gravity: A comprehensive review. *Rept Prog Phys* 83(7):075901, DOI 10.1088/1361-6633/ab12bc, [1807.01699](#)
- [124] Levi M, Steinhoff J (2016) Complete conservative dynamics for inspiralling compact binaries with spins at fourth post-Newtonian order. arXiv e-prints arXiv:1607.04252, [1607.04252](#)

- [125] Lidov ML (1962) The evolution of orbits of artificial satellites of planets under the action of gravitational perturbations of external bodies. *Planetary and Space Science* 9(10):719–759, DOI 10.1016/0032-0633(62)90129-0
- [126] LIGO Scientific Collaboration (2018) LIGO Algorithm Library - LAL-Suite. free software (GPL), DOI 10.7935/GT1W-FZ16, URL <https://lscsoft.docs.ligo.org/lalsuite/lalsimulation/index.html>
- [127] London L, Khan S, Fauchon-Jones E, García C, Hannam M, Husa S, Jiménez-Forteza X, Kalaghatgi C, Ohme F, Pannarale F (2018) First higher-multipole model of gravitational waves from spinning and coalescing black-hole binaries. *Phys Rev Lett* 120(16):161102, DOI 10.1103/PhysRevLett.120.161102, [1708.00404](#)
- [128] Lorimer DR (2005) Binary and millisecond pulsars. *Living Rev Rel* 8:7, DOI 10.12942/lrr-2005-7, [astro-ph/0511258](#)
- [129] Maggiore M (2007) *Gravitational Waves. Vol. 1: Theory and Experiments.* Oxford Master Series in Physics, Oxford University Press
- [130] Marsat S (2015) Cubic order spin effects in the dynamics and gravitational wave energy flux of compact object binaries. *Class Quant Grav* 32(8):085008, DOI 10.1088/0264-9381/32/8/085008, [1411.4118](#)
- [131] van de Meent M, Pfeiffer HP (2020) Intermediate mass-ratio black hole binaries: Applicability of small mass-ratio perturbation theory. *Phys Rev Lett* 125(18):181101, DOI 10.1103/PhysRevLett.125.181101, [2006.12036](#)
- [132] Mei J, et al (2020) The TianQin project: current progress on science and technology. *arXiv e-prints arXiv:2008.10332*, [2008.10332](#)
- [133] Michimura Y, et al (2019) Prospects for improving the sensitivity of KAGRA gravitational wave detector. In: 15th Marcel Grossmann Meeting on Recent Developments in Theoretical and Experimental General Relativity, Astrophysics, and Relativistic Field Theories (MG15) Rome, Italy, July 1-7, 2018, [1906.02866](#)
- [134] Mino Y, Sasaki M, Shibata M, Tagoshi H, Tanaka T (1997) Black hole perturbation: Chapter 1. *Prog Theor Phys Suppl* 128:1–121, DOI 10.1143/PTPS.128.1, [gr-qc/9712057](#)
- [135] Mishra CK, Kela A, Arun K, Faye G (2016) Ready-to-use post-Newtonian gravitational waveforms for binary black holes with nonprecessing spins: An update. *Phys Rev D* 93(8):084054, DOI 10.1103/PhysRevD.93.084054, [1601.05588](#)
- [136] Moore B, Yunes N (2019) A 3PN Fourier Domain Waveform for Non-Spinning Binaries with Moderate Eccentricity. *Class Quant Grav* 36(18):185003, DOI 10.1088/1361-6382/ab3778, [1903.05203](#)
- [137] Moore B, Favata M, Arun K, Mishra CK (2016) Gravitational-wave phasing for low-eccentricity inspiralling compact binaries to 3PN order. *Phys Rev D* 93(12):124061, DOI 10.1103/PhysRevD.93.124061, [1605.00304](#)
- [138] Moore B, Robson T, Loutrel N, Yunes N (2018) Towards a Fourier domain waveform for non-spinning binaries with arbitrary eccentricity. *Class Quant Grav* 35(23):235006, DOI 10.1088/1361-6382/aaea00, [1807.07163](#)

- [139] Nagar A, Messina F, Rettegno P, Bini D, Damour T, Geralico A, Akcay S, Bernuzzi S (2019) Nonlinear-in-spin effects in effective-one-body waveform models of spin-aligned, inspiralling, neutron star binaries. *Phys Rev D* 99(4):044007, DOI 10.1103/PhysRevD.99.044007, [1812.07923](#)
- [140] Nagar A, Riemenschneider G, Pratten G, Rettegno P, Messina F (2020) Multipolar effective one body waveform model for spin-aligned black hole binaries. *Phys Rev D* 102(2):024077, DOI 10.1103/PhysRevD.102.024077, [2001.09082](#)
- [141] Nagar A, Rettegno P, Gamba R, Bernuzzi S (2021) Effective-one-body waveforms from dynamical captures in black hole binaries. *Phys Rev D* 103(6):064013, DOI 10.1103/PhysRevD.103.064013, [2009.12857](#)
- [142] Nagar A, et al (2018) Time-domain effective-one-body gravitational waveforms for coalescing compact binaries with nonprecessing spins, tides and self-spin effects. *Phys Rev D* 98(10):104052, DOI 10.1103/PhysRevD.98.104052, [1806.01772](#)
- [143] Nakamura T, Oohara K, Kojima Y (1987) General Relativistic Collapse to Black Holes and Gravitational Waves from Black Holes. *Prog Theor Phys Suppl* 90:1–218, DOI 10.1143/PTPS.90.1
- [144] Nakamura T, et al (2016) Pre-DECIGO can get the smoking gun to decide the astrophysical or cosmological origin of GW150914-like binary black holes. *PTEP* 2016(9):093E01, DOI 10.1093/ptep/ptw127, [1607.00897](#)
- [145] Narikawa T, Uchikata N, Kawaguchi K, Kiuchi K, Kyutoku K, Shibata M, Tagoshi H (2020) Reanalysis of the binary neutron star mergers GW170817 and GW190425 using numerical-relativity calibrated waveform models. *Phys Rev Res* 2(4):043039, DOI 10.1103/PhysRevResearch.2.043039, [1910.08971](#)
- [146] Nollert HP (1999) TOPICAL REVIEW: Quasinormal modes: the characteristic ‘sound’ of black holes and neutron stars. *Class Quant Grav* 16:R159–R216, DOI 10.1088/0264-9381/16/12/201
- [147] Ossokine S, et al (2020) Multipolar Effective-One-Body Waveforms for Precessing Binary Black Holes: Construction and Validation. *Phys Rev D* 102(4):044055, DOI 10.1103/PhysRevD.102.044055, [2004.09442](#)
- [148] Pan Y, Buonanno A, Boyle M, Buchman LT, Kidder LE, Pfeiffer HP, Scheel MA (2011) Inspiral-merger-ringdown multipolar waveforms of nonspinning black-hole binaries using the effective-one-body formalism. *Phys Rev D* 84:124052, DOI 10.1103/PhysRevD.84.124052, [1106.1021](#)
- [149] Pan Y, Buonanno A, Fujita R, Racine E, Tagoshi H (2011) Post-Newtonian factorized multipolar waveforms for spinning, non-precessing black-hole binaries. *Phys Rev D* 83:064003, DOI 10.1103/PhysRevD.83.064003, [Erratum: *Phys.Rev.D* 87, 109901 (2013)], [1006.0431](#)
- [150] Pan Y, Buonanno A, Taracchini A, Kidder LE, Mroué AH, Pfeiffer HP, Scheel MA, Szilágyi B (2014) Inspiral-merger-ringdown waveforms of spinning, precessing black-hole binaries in the effective-one-body formalism. *Phys Rev D* 89(8):084006, DOI 10.1103/PhysRevD.89.084006, [1307.6232](#)



- [151] Pani P, Gualtieri L, Ferrari V (2015) Tidal Love numbers of a slowly spinning neutron star. *Phys Rev D* 92(12):124003, DOI 10.1103/PhysRevD.92.124003, [1509.02171](#)
- [152] Peters P (1964) Gravitational Radiation and the Motion of Two Point Masses. *Phys Rev* 136:B1224–B1232, DOI 10.1103/PhysRev.136.B1224
- [153] Poisson E (1998) Gravitational waves from inspiraling compact binaries: The Quadrupole moment term. *Phys Rev D* 57:5287–5290, DOI 10.1103/PhysRevD.57.5287, [gr-qc/9709032](#)
- [154] Poisson E (2004) Absorption of mass and angular momentum by a black hole: Time-domain formalisms for gravitational perturbations, and the small-hole / slow-motion approximation. *Phys Rev D* 70:084044, DOI 10.1103/PhysRevD.70.084044, [gr-qc/0407050](#)
- [155] Poisson E (2015) Tidal deformation of a slowly rotating black hole. *Phys Rev D* 91(4):044004, DOI 10.1103/PhysRevD.91.044004, [1411.4711](#)
- [156] Poisson E, Sasaki M (1995) Gravitational radiation from a particle in circular orbit around a black hole. 5: Black hole absorption and tail corrections. *Phys Rev D* 51:5753–5767, DOI 10.1103/PhysRevD.51.5753, [gr-qc/9412027](#)
- [157] Poisson E, Will CM (2014) *Gravity*. Cambridge University Press, Cambridge, UK
- [158] Porto RA (2016) The effective field theorist approach to gravitational dynamics. *Phys Rept* 633:1–104, DOI 10.1016/j.physrep.2016.04.003, [1601.04914](#)
- [159] Pratten G, Husa S, Garcia-Quiros C, Colleoni M, Ramos-Buades A, Estelles H, Jaume R (2020) Setting the cornerstone for the IMRPhenomX family of models for gravitational waves from compact binaries: The dominant harmonic for non-precessing quasi-circular black holes. *Phys Rev D* 102(6):064001, DOI 10.1103/PhysRevD.102.064001, [2001.11412](#)
- [160] Pratten G, et al (2021) Computationally efficient models for the dominant and subdominant harmonic modes of precessing binary black holes. *Phys Rev D* 103(10):104056, DOI 10.1103/PhysRevD.103.104056, [2004.06503](#)
- [161] Pretorius F (2005) Evolution of binary black hole spacetimes. *Phys Rev Lett* 95:121101, DOI 10.1103/PhysRevLett.95.121101, [gr-qc/0507014](#)
- [162] Pürrer M (2014) Frequency domain reduced order models for gravitational waves from aligned-spin compact binaries. *Class Quant Grav* 31(19):195010, DOI 10.1088/0264-9381/31/19/195010, [1402.4146](#)
- [163] Reitze D, et al (2019) Cosmic Explorer: The U.S. Contribution to Gravitational-Wave Astronomy beyond LIGO. *Bull Am Astron Soc* 51:035, [1907.04833](#)
- [164] Rifat NE, Field SE, Khanna G, Varma V (2020) Surrogate model for gravitational wave signals from comparable and large-mass-ratio black hole binaries. *Phys Rev D* 101(8):081502, DOI 10.1103/PhysRevD.101.081502, [1910.10473](#)
- [165] Sago N, Fujita R, Nakano H (2016) Accuracy of the Post-Newtonian Approximation for Extreme-Mass Ratio Inspirals from Black-hole Perturbation

- Approach. *Phys Rev D* 93(10):104023, DOI 10.1103/PhysRevD.93.104023, [1601.02174](#)
- [166] Santamaria L, et al (2010) Matching post-Newtonian and numerical relativity waveforms: systematic errors and a new phenomenological model for non-precessing black hole binaries. *Phys Rev D* 82:064016, DOI 10.1103/PhysRevD.82.064016, [1005.3306](#)
- [167] Sasaki M, Tagoshi H (2003) Analytic black hole perturbation approach to gravitational radiation. *Living Rev Rel* 6:6, DOI 10.12942/lrr-2003-6, [gr-qc/0306120](#)
- [168] Schmidt P, Hannam M, Husa S (2012) Towards models of gravitational waveforms from generic binaries: A simple approximate mapping between precessing and non-precessing inspiral signals. *Phys Rev D* 86:104063, DOI 10.1103/PhysRevD.86.104063, [1207.3088](#)
- [169] Schäfer G, Jaranowski P (2018) Hamiltonian formulation of general relativity and post-Newtonian dynamics of compact binaries. *Living Rev Rel* 21(1):7, DOI 10.1007/s41114-018-0016-5, [1805.07240](#)
- [170] Sesana A (2016) Prospects for Multiband Gravitational-Wave Astronomy after GW150914. *Phys Rev Lett* 116(23):231102, DOI 10.1103/PhysRevLett.116.231102, [1602.06951](#)
- [171] Seto N, Kawamura S, Nakamura T (2001) Possibility of direct measurement of the acceleration of the universe using 0.1-Hz band laser interferometer gravitational wave antenna in space. *Phys Rev Lett* 87:221103, DOI 10.1103/PhysRevLett.87.221103, [astro-ph/0108011](#)
- [172] Szilágyi B, Blackman J, Buonanno A, Taracchini A, Pfeiffer HP, Scheel MA, Chu T, Kidder LE, Pan Y (2015) Approaching the Post-Newtonian Regime with Numerical Relativity: A Compact-Object Binary Simulation Spanning 350 Gravitational-Wave Cycles. *Phys Rev Lett* 115(3):031102, DOI 10.1103/PhysRevLett.115.031102, [1502.04953](#)
- [173] Tagoshi H, Mano S, Takasugi E (1997) PostNewtonian expansion of gravitational waves from a particle in circular orbits around a rotating black hole: Effects of black hole absorption. *Prog Theor Phys* 98:829–850, DOI 10.1143/PTP.98.829, [gr-qc/9711072](#)
- [174] Tanay S, Haney M, Gopakumar A (2016) Frequency and time domain inspiral templates for comparable mass compact binaries in eccentric orbits. *Phys Rev D* 93(6):064031, DOI 10.1103/PhysRevD.93.064031, [1602.03081](#)
- [175] Taracchini A, Pan Y, Buonanno A, Barausse E, Boyle M, Chu T, Lovelace G, Pfeiffer HP, Scheel MA (2012) Prototype effective-one-body model for nonprecessing spinning inspiral-merger-ringdown waveforms. *Phys Rev D* 86:024011, DOI 10.1103/PhysRevD.86.024011, [1202.0790](#)
- [176] Taracchini A, et al (2014) Effective-one-body model for black-hole binaries with generic mass ratios and spins. *Phys Rev D* 89(6):061502, DOI 10.1103/PhysRevD.89.061502, [1311.2544](#)
- [177] Thompson JE, Fauchon-Jones E, Khan S, Nitoglia E, Pannarale F, Dietrich T, Hannam M (2020) Modeling the gravitational wave signature of neutron

- star black hole coalescences: PhenomNSBH. *Phys Rev D* 101:124059, DOI 10.1103/PhysRevD.101.124059, [2002.08383](#)
- [178] Tiwari S, Gopakumar A (2020) Combining post-circular and Padé approximations to compute Fourier domain templates for eccentric inspirals. *Phys Rev D* 102(8):084042, DOI 10.1103/PhysRevD.102.084042, [2009.11333](#)
- [179] Tiwari S, Achamveedu G, Haney M, Hemantakumar P (2019) Ready-to-use Fourier domain templates for compact binaries inspiraling along moderately eccentric orbits. *Phys Rev D* 99(12):124008, DOI 10.1103/PhysRevD.99.124008, [1905.07956](#)
- [180] Varma V, Field SE, Scheel MA, Blackman J, Gerosa D, Stein LC, Kidder LE, Pfeiffer HP (2019) Surrogate models for precessing binary black hole simulations with unequal masses. *Phys Rev Research* 1:033015, DOI 10.1103/PhysRevResearch.1.033015, [1905.09300](#)
- [181] Vitale S (2016) Multiband Gravitational-Wave Astronomy: Parameter Estimation and Tests of General Relativity with Space- and Ground-Based Detectors. *Phys Rev Lett* 117(5):051102, DOI 10.1103/PhysRevLett.117.051102, [1605.01037](#)
- [182] Yunes N, Berti E (2008) Accuracy of the post-Newtonian approximation: Optimal asymptotic expansion for quasicircular, extreme-mass ratio inspirals. *Phys Rev D* 77:124006, DOI 10.1103/PhysRevD.77.124006, 10.1103/PhysRevD.83.109901, [Erratum: *Phys. Rev.D*83,109901(2011)], [0803.1853](#)
- [183] Yunes N, Pretorius F (2009) Fundamental Theoretical Bias in Gravitational Wave Astrophysics and the Parameterized Post-Einsteinian Framework. *Phys Rev D* 80:122003, DOI 10.1103/PhysRevD.80.122003, [0909.3328](#)
- [184] Zhang Z, Yunes N, Berti E (2011) Accuracy of the post-Newtonian approximation. II. Optimal asymptotic expansion of the energy flux for quasicircular, extreme mass-ratio inspirals into a Kerr black hole. *Phys Rev D* 84:024029, DOI 10.1103/PhysRevD.84.024029, [1103.6041](#)